New analytical model for the ozone electronic ground state potential surface and accurate *ab initio* vibrational predictions at high energy range

Vladimir G. Tyuterev,[1,a)] Roman V. Kochanov,[1,2] Sergey A. Tashkun,[2] Filip Holka,[3] and Péter G. Szalay[4]

[1]*Groupe de Spectrométrie Moléculaire et Atmosphérique UMR CNRS 7331, UFR Sciences BP 1039, 51687 Reims Cedex 2, France*
[2]*Laboratory of Theoretical Spectroscopy, V.E. Zuev Institute of Atmospheric Optics SB RAS 1, Akademician Zuev square, 634021 Tomsk, Russia*
[3]*Slovak University of Technology, Paulinska 16, 917 24 Trnava, Slovak Republic*
[4]*Institute of Chemistry, Eötvös University, H-1117 Budapest, Pázmány sétány 1/A, Hungary*

(Received 4 June 2013; accepted 4 September 2013; published online 4 October 2013)

An accurate description of the complicated shape of the potential energy surface (PES) and that of the highly excited vibration states is of crucial importance for various unsolved issues in the spectroscopy and dynamics of ozone and remains a challenge for the theory. In this work a new analytical representation is proposed for the PES of the ground electronic state of the ozone molecule in the range covering the main potential well and the transition state towards the dissociation. This model accounts for particular features specific to the ozone PES for large variations of nuclear displacements along the minimum energy path. The impact of the shape of the PES near the transition state (existence of the "reef structure") on vibration energy levels was studied for the first time. The major purpose of this work was to provide accurate theoretical predictions for ozone vibrational band centres at the energy range near the dissociation threshold, which would be helpful for understanding the very complicated high-resolution spectra and its analyses currently in progress. Extended *ab initio* electronic structure calculations were carried out enabling the determination of the parameters of a minimum energy path PES model resulting in a new set of theoretical vibrational levels of ozone. A comparison with recent high-resolution spectroscopic data on the vibrational levels gives the root-mean-square deviations below 1 cm^{-1} for ozone band centres up to 90% of the dissociation energy. New *ab initio* vibrational predictions represent a significant improvement with respect to all previously available calculations. © *2013 AIP Publishing LLC*. [http://dx.doi.org/10.1063/1.4821638]

I. INTRODUCTION

During past decades the spectroscopy and dynamics of ozone has been the subject of numerous studies because of the well-known role this molecule plays in atmospheric physics and climate processes. Despite considerable advances in both experiment and modeling, several issues related to the ozone properties are still unresolved.[1] Ozone in its excited quantum states and the related processes of ozone recombination remain a puzzle for the fundamental molecular physics. One of the challenging problems is the interpretation of the anomalous isotope enrichment in atmospheric ozone which is linked to the formation reaction and thus to the molecular dynamics at the dissociation limit (see, e.g., Mauersberger *et al.*,[2] Thiemens,[3] Hippler *et al.*,[4] Janssen *et al.*,[5] Gao and Marcus,[6,7] Grebenshchikov and Schinke,[8] Dawes *et al.*,[9] and references therein). For most molecules the isotope enrichment scales with relative mass differences, but the case of ozone shows extremely marked deviation from this rule as was observed in the troposphere, in the stratosphere, and also in laboratory experiments.

The accurate determination of the 3D ozone potential energy surfaces (PES) is a prerequisite for both theoretical calculations of the complex kinetics of the formation, dissociation, energy transfer, and recombination of the ozone molecule[1–11] and for spectra analyses[12–19] at high energy range approaching the dissociation threshold. The ozone molecule exhibits a complex electronic structure and represents a challenge for accurate *ab initio* calculations, hence we lack information for the understanding the unusual shape of the PES. The ground state PES of ozone has several potential minima separated by barriers.[1,20–23] The three lowest identical shallow wells of C_{2V} local symmetry correspond to nuclear permutations (open ozone structure with apex angle of ∼117° and the equilibrium bond length ∼2.4 a.u.). The ring D_{3h} minimum[22] is located 0.3 eV above the O_2 ($^3\Sigma_g^-$) + $O(^3P)$ dissociation threshold and is thus less important for dynamical and spectroscopical applications.

Considerable effort has been devoted to the determination of PES in the X^1A_1 ground electronic state by *ab initio* calculations[20–35] or by fitting to experimental rovibrational data.[36–38] Global 3D ozone surfaces designed for dynamical calculations have been constructed by Yamashita *et al.*[24] and more accurately by Siebert, Schinke, and Bittererova[20,21] (the corresponding PES is usually referred to as SSB PES). The

a)Author to whom correspondence should be addressed. Electronic mail: vladimir.tyuterev@univ-reims.fr. Telephone: +33 326913380.

latter one has been built with spline interpolations of *ab initio* electronic energies on the extensive grid of 5000 nuclear configurations. The remaining questions concern the controversial issues related to the shape of the PES at the transition state (TS) and the underestimated value of the dissociation limit. Earlier *ab initio* calculations[20–27] predicted an activation barrier at the entrance of the dissociation channel at $r_1 \sim 3.8$–4.0 a.u. with the other bond length $r_2 \sim 2.28$ a.u. close to the equilibrium bond length of the O_2 fragment with the apex angle $\theta \sim 115°$–$117°$ close to the equilibrium value of the open ozone structure. Additionally, a shallow van der Waals (vdW) minimum along the dissociation reaction coordinate at $r_1 \sim 4.5$–5.0 a.u. has been predicted.

Various 1D and 2D calculations at higher level of the electronic structure calculations have suggested that the minimum energy path (MEP) shape has a "reef"-like structure[29,31,32] with a submerged barrier below the dissociation limit. Following previous studies by Fleurat-Lessard *et al.*[32] this "reef" feature was incorporated into a so-called "hybrid PES" by Babikov *et al.*[10] by introducing a correction to the SSB PES[20,21] with empirical adjustments to match the experimental dissociation energy. The modified SSB surface has been used to study the metastable states[10] and the van der Waals states.[39–41] *Ab initio* studies of the electronic ground state (GS) of ozone have been recently reviewed by Holka *et al.*[33] In addition, using 1D and 2D PES cuts near the transition state towards the dissociation, they also presented a detailed investigation of various ingredients of the electronic structure methods: role of size-consistency and relativistic corrections, as well as basis set effects including extrapolation to the complete basis set limit. Long range behavior of the potential has been discussed by Lepers *et al.*[34] Excited electronic ozone states have been considered in series of papers[30,42–45] and reviewed by Grebenshchikov *et al.*[46]

The important impact of the barrier height and the depth of the vdW minimum on the dynamics of the formation and fragmentation of the excited ozone molecule have been discussed in several studies.[1,8–11,39–41] All previous studies suggested that rate coefficient of the $O + O_2$ exchange reaction are very sensitive to the shape of the PES in the TS region[1] and one of the major obstacles in our understanding of the ozone kinetics is the lack of a quantitatively accurate PES.[9] Recently, Dawes *et al.*[9] have argued that an accurate account for several interacting electronic states in the TS region should result in a ground state potential function without the "reef" feature found in previous *ab initio* calculations. They have computed a 2D surface at the TS region by including 13 singlet states in a state averaged complete active space self-consistent field calculations and were able to derive the thermal rate constant for the exchange reaction using a quantum statistical model that showed a much better agreement with kinetic experimental data. They also concluded that exact quantum dynamics calculations require a full-dimensional PES.

The focus of our work is to obtain a realistic full dimensional ozone PES model in the range important for both spectroscopy and dynamics applications. This range of nuclear configurations involves the main C_{2V} potential well, and the transition states along the minimum energy path towards the dissociation. The primary aim is an accurate prediction of highly excited vibration states near the dissociation threshold. An access of these states would be crucial for checking the shape of the PES in the TS region and verifying quantum-mechanical nuclear motion calculations.[1,8,18,19,21,36,37] There are at least three important fields of applications, which could be considered in this context.

The first one concerns the analyses of high-resolution spectra in the range just below the dissociation energy using the very sensitive laser Cavity-Ring-Down-Spectroscopy (CRDS) measurements by Kassi and Campargue *et al.*[12,13] These analyses are currently in progress, see works by Barbe *et al.*[14–19,48] Until recently, spectral analyses relied on empirical potentials. The most accurate empirical PES for the spectroscopic calculations near the open ozone configuration have been determined by Tyuterev *et al.*[36,37] from the fit to experimental vibration–rotation data of $^{16}O_3$ below 5800 cm^{-1}. This PES has been used for the assignment of CRDS spectra[13–19] of $^{16}O_3$ and $^{18}O_3$ and for the extrapolation towards highly excited vibrational states.[18] Calculations for spectroscopic applications and the vibrational assignment have been done by two complementary independent methods. One uses variational calculations in internal bond length-bond angle coordinates following Refs. 36, 37, and 47, the second one employed the method of high order Contact Transformations (CT) in normal coordinates[49–51] providing normal mode assignments for all bands. The band center predictions using this PES have been found accurate in average within 1 cm^{-1} both for $^{16}O_3$ and $^{18}O_3$ observations[13,15,19] up to 7000 cm^{-1}, but appeared considerably less reliable at higher energy range. This presumably happened because a simple Morse-cosine expansion was not the most appropriate one to describe the complicated shape of the PES at the TS range. Despite a significant progress[13–19] a substantial number of observed vibration-rotational lines have not yet been assigned, and numerous vibration states have been considered as "dark" states though the corresponding bands are symmetry allowed. Also, more accurate predictions for the metastable ro-vibrational states above the dissociation limit are required to find "doorway" state for the ozone dissociation from low-lying excited electronic states in order to make a reliable interpretation of broad features in observed absorption spectra (Mondelain *et al.*[18]).

The second issue concerns a theoretical calculation of the coupling parameters for multiple anharmonic and Coriolis resonances which are very pronounced in ozone spectra. It has been recently shown[52] that this information derived from a PES via the CT method is useful for a reliable spectroscopic data reduction in the range around 3000 cm^{-1}. In this case again, an empirical PES[38] was used which was valid at moderate energies only. An extension of this promising approach to assign the complicated spectra near the dissociation threshold or to describe intensity borrowing effects in hybrid bands[53–56] of asymmetric ozone isotopologues requires more accurate models for the 3D PES.

The third possible application is a prediction of cascades of radiative transitions for multi-photon laser experiments (in a similar way as was done for the water molecule[57] that allowed obtaining a wealth of new experimental data

otherwise inaccessible) or for a correct account of non-local thermodynamic equilibrium effects[58,59] in the modelling of emission and absorption properties of the middle and upper atmosphere.

In this work we propose a new analytical representation of the ozone PES in the range from the main well and along the MEP towards the dissociation, which could have certain advantages compared to spline-type procedures. It is expected to be more robust with respect to outliers (present due to convergence problems) in *ab initio* energies and for evaluation of PES derivatives, if the number of parameters is much less than the number of fitted points. On the other hand, it can be more easily converted to spectroscopic effective models using CT method[49–51] for ro-vibrational assignments and for the computation of coupling parameters. However, finding an appropriate analytical shape of the ozone PES is quite challenging. Apart from the above-mentioned issue concerning the possible reef structure at the TS, the shape of ozone PES possesses other peculiarities. Contrary to other triatomics such as H_2O, the ozone fragmentation energy is not additive (Sec. IV), and the MEP is not rectilinear on the way from the equilibrium to the dissociation. Quite dense grid of *ab initio* points was necessary to investigate these features and to find an appropriate parameterisation.

The paper is structured as follows. In Sec. II extensive electronic structure calculations on a dense 3D grid of nuclear configurations are described. The impact of the complete basis set (CBS) extrapolation on vibration frequencies and the issues concerning the reef structure are discussed in Sec. III. The new analytical MEP model is described in Sec. IV while the fit to *ab initio* points is presented in Sec. V for two versions of the ozone PES: one with the reef structure on the MEP, and another without the reef structure using corrections due to the work of Dawes *et al.*[9] Section VI is devoted to variational and discrete-variable-representation (DVR) nuclear motion calculations. A comparison of predictions with experimental band centres derived from all available high-resolution spectra analyses is given in Secs. VII and VIII is devoted to the discussion of results.

II. *AB INITIO* ELECTRONIC STRUCTURE CALCULATIONS

Accurate *ab initio* prediction of the PES and molecular properties for small molecules helps resolving many issues related to the analyses of the spectra and much progress has been achieved in last years in this respect (see, for example, Refs. 60–75 and references therein, the list being not exhaustive).

Because of the complexity of the electronic structure, this still remains a formidable challenge in the case of ozone. While a multiconfigurational (MC) version of *ab initio* methods is always needed for bond dissociation, due to some near degeneracy occurring between the HOMO (highest occupied molecular orbital) and LUMO (lowest unoccupied molecular orbital) of ozone, MC description is necessary already near equilibrium.[23,28] In addition, quantitative results on the PES can be hoped only if dynamic correlation effects[27–33] are also included. The latter can be accounted for by using multireference configuration interaction (MRCI) method (for a recent review see Ref. 76) or it size-consistency corrected variant, the multireference averaged quadratic coupled cluster (MR-AQCC) method by Szalay and Bartlett.[77] Using this type of methodology, it was possible to cover all vibration levels up to the dissociation limit with an accuracy of 1 or 2 cm^{-1} for the light molecule LiH.[70,71] In the case of ozone further approximation needs to be introduced: it is possible to significantly reduce the computational requirements by using the so called "internally contracted" (ic) versions[78,79] of multireference methods (for example ic-MRCI or ic-MR-AQCC), but one has to remember that the flexibility of the method is greatly compromised by this approximation. The absolute majority of ozone calculations so far used internal contraction.[20–22,27–35] The most straightforward choice for reference space is a CAS (complete active space) where one selects the "most important" orbitals (active orbitals) and distributes the "most important" electrons (active electrons) among these. Technically, CAS is denoted by CAS(m,n), where m is number of active electrons and n is the number of active orbitals. From the chemical point of view, considering valence orbitals and electrons as "most important" is a well defined, unambiguous, and safe choice. Unfortunately, this often leads to too large *ansätze* and therefore some simplification is necessary. The reference space has two roles: (a) it defines the MCSCF (multiconfiguration wave function, often termed as CASSCF) used to obtain the orbitals and (b) it is used to generate the CI expansion space by applying singe and double replacements on it.

As of the basis for the molecular orbital, accurate calculations often use the hierarchical basis sets by Dunning, termed as correlation consistent basis sets (cc-pVXZ)[80] depending on the cardinal number X (= D, T, Q, 5, 6, . . .). In addition, basis set extrapolation schemes are often used to speed-up convergence: the most popular extrapolation formula is based on an X^{-3} dependence of the complete basis set (CBS) energy on the cardinal number:[84,85]

$$E^X = E^{CBS} + const/X^3. \quad (1)$$

The cc-pVXZ basis can be augmented by diffuse functions (aug-cc-pVXZ sets; will be denoted by AVXZ in what follows) or by functions describing the core electrons (cc-pCVXZ sets; denoted as CVXZ below).

In case of ozone, sections of the PES have been calculated by Xantheas *et al.*,[23] Banichevich *et al.*,[25] Borowski *et al.*,[26] Müller *et al.*,[27] Xie *et al.*,[28] who have studied open (C_{2V}) and ring (D_{3h}) structures as well as dissociation energy at various levels of the theory. A very significant progress in the *ab initio* calculations for a large range of internuclear distances for the ozone PES has been achieved by the group of Schinke and co-workers.[1,20,21,30–32] For the construction of the most extended presently available global electronic ground states ozone PES Siebert *et al.*[20,21] have used ic-MRCI method with CAS reference functions and quadruple zeta correlation consistent basis set (cc-pVQZ).[80] The complete active space used by Siebert *et al.*[20,21] corresponds to CAS(12,9): that is 12 electrons in 9 orbitals including just the 2p orbitals of oxygen atoms. In the subsequent ic-MRCI calculations the 1s core electrons were not correlated.

Size-consistency error has been corrected by Davidson correction.[81] The key advantage of the resulting SSB global PES[20,21] is that this surface covers nearly the entire range of nuclear configurations by using the spline interpolation obtained from a regular grid of ~5000 *ab initio* points. This also provided correct values of vibration energies, at least for low and medium vibrational excitations. For this reason the SSB PES or somewhat modified versions of this PES[10,32] have been used in most of studies on ozone dynamics. However, interpretations of current spectroscopic experiments on highly excited vibration-rotation states near the dissociation threshold[13–19] require more accurate 3D *ab initio* PES. One of the reasons is that the global, fully *ab initio* PES[20,21] underestimated the GS dissociation limit by more than 800 cm^{-1} presumably because of insufficiency of the cc-pVQZ basis set. In addition it seems also be important that the TS range should be more thoroughly investigated.[9,33]

In this work we extended electronic structure calculations in line with our previous study.[33] A larger complete active space of orbitals was used and more than ten different versions of *ab initio* ansätze involving various electronic basis sets and calculation methods were tested. In most of the present calculations we used ic-MRCI method with augmented valence correlation consistent basis sets (AVXZ). In order to investigate the convergence of vibration frequencies with respect to the atomic basis set we computed 3D surfaces for cardinal numbers X = T, Q, 5, 6 that is for triple-, quadruple-, quintuple-, and sextuple zeta AVXZ sets. The size of these sets grows cubically with the cardinal number X. In case of X = 6 the contribution up to *i*-orbitals ($l = 6$) were included.[82]

The ic-MR-CISD electronic wave functions were built on the top of the CAS (18,12) reference space, i.e., the active space consists of the 2s and 2p atomic orbitals of oxygen, and hence it is a full valence space. In the ansatz denoted as $a1$ the orbitals were obtained in the MCSCF procedure with the CAS(18,12) space (CASSCF (18,12)); the three 1s orbitals are kept doubly occupied in this ansatz, but they are optimized. On the other hand, in the ansatz referred to as $a5$ a different procedure to obtain orbitals had to be adopted due to some instability issues at the TS and on the way to dissociation above $r = 4$ or 5 a.u. Here the orbitals were obtained in a two-step procedure: in the first step a CASSCF (12,9) wave function was used with 2p orbitals active, while 1s and 2s orbitals double occupied but optimized. Using the resulting orbitals, a CASSCF (18,12) calculation was performed with both 2s and 2p orbitals active, but 1s orbitals frozen, i.e., these core orbitals retain there form from the smaller CASSCF calculations. In both $a1$ and $a5$ ansätze dynamic correlation was considered by including all single and double excitations out of the CAS (18,12) reference functions in an ic-MR-CISD procedure and the frozen core approximation was adopted. This resulted in up to about 26.7×10^6 configurations with the largest basis set.

In all of our calculations the CI energy was augmented by Davidson-type corrections[81] ($+Q_D$) in order to minimize the size-consistency error. For a validation we have also computed representative series of points with the ic-MR-AQCC method.[77] Within the main well the ic-MR-AQCC gave very similar results though it required nearly twice as much iterations to converge. Relativistic corrections were not included in our calculations because they were found to be small compared to other contributions which were necessary to account for. The reader is referred to Ref. 33 for a detailed discussion of various *ab initio* corrections and for the review of issues concerning electronic structure methods in case of the ozone ground state. All of the electronic structure calculations were carried out with the MOLPRO suite of *ab initio* programs.[83]

In this work we essentially focus on two ranges of nuclear configurations. The first one is usually called "spectroscopically accessible region." By this we mean a volume of geometrical configuration space in the main C_{2V} potential well, which could be sampled by the rotation–vibration wave functions corresponding to transitions observed by the available spectroscopic experiments. To cover this range we generated a dense grid of configurations for ansatz $a1$ with the distances varied from 1.8 to 4.5 a.u. and the angles from 94° to 145°. The grid step size was not regular with respect to nuclear displacements but was chosen according to the energy change: near the equilibrium, up to $E\text{-}E_0 < 5000\ cm^{-1}$ we used in average $\Delta r = 0.05$ a.u. and $\Delta\theta = 2°$, whereas the step increased to $\Delta r = 0.1$ a.u. and $\Delta\theta = 5°$ up to $E\text{-}E_0 < 14\,000\ cm^{-1}$ and to $\Delta r = 0.2$ a.u. for r >3 a.u. (here E_0 is the energy at the reference nuclear configuration $r_1 = r_2 = 2.4$ a.u., $\theta = 117°$). In addition, we computed sparser series for θ from 70° to 175°. The most representative PES in this first range corresponds to 1950 nuclear configurations computed with the ic-MRCI based on $a1$ ansatz using AV5Z basis. The second range covers the nuclear configurations around the MEP from the main C_{2V} well towards TS and continuing to dissociation (up to R = 12 a.u.). In this range we computed the PES at about 1800 points with the ic-MRCI based on $a5$ ansatz using again the AV5Z basis set.

In order to study the dependence of the PES on cardinal number X of the basis and to extrapolate the PES to the CBS limit both in the main potential well and in the dissociation channel, we also calculated electronic energies with AVTZ, AVQZ, and AV6Z basis sets on sparser grids of 1050, 1050, and 690 points, respectively, for the above-mentioned two regions. A 3D comparison of the results obtained with AV5Z and AV6Z basis sets is shown in Figure 1. Calculations with X = 6 (right-hand side) are more demanding and thus sample a sparser grid than that of X = 5 (left-hand side). The panels p1, p2 correspond to the range near the main equilibrium up to $5000\ cm^{-1}$, where we have eight times denser grid computed at the AV5Z level compared to previously available 3D SSB calculations[20,21] at the cc-pVQZ level. The panels p3 and p4 correspond to the *ab initio* calculations at the TS range, and the panels p5 and p6 to the PES points up to $14\,000\ cm^{-1}$.

III. DEPENDENCE OF HARMONIC FREQUENCIES ON THE CARDINAL NUMBER AND THE PES SHAPE AT THE TS TOWARDS THE DISSOCIATION

Using the calculated *ab initio* energies we computed, as a first step, the harmonic vibration frequencies ω_i of $^{16}O_3$ for various cardinal numbers of the electronic basis set (X = T, Q, 5, 6) and also for the CBS limit. For the latter we have

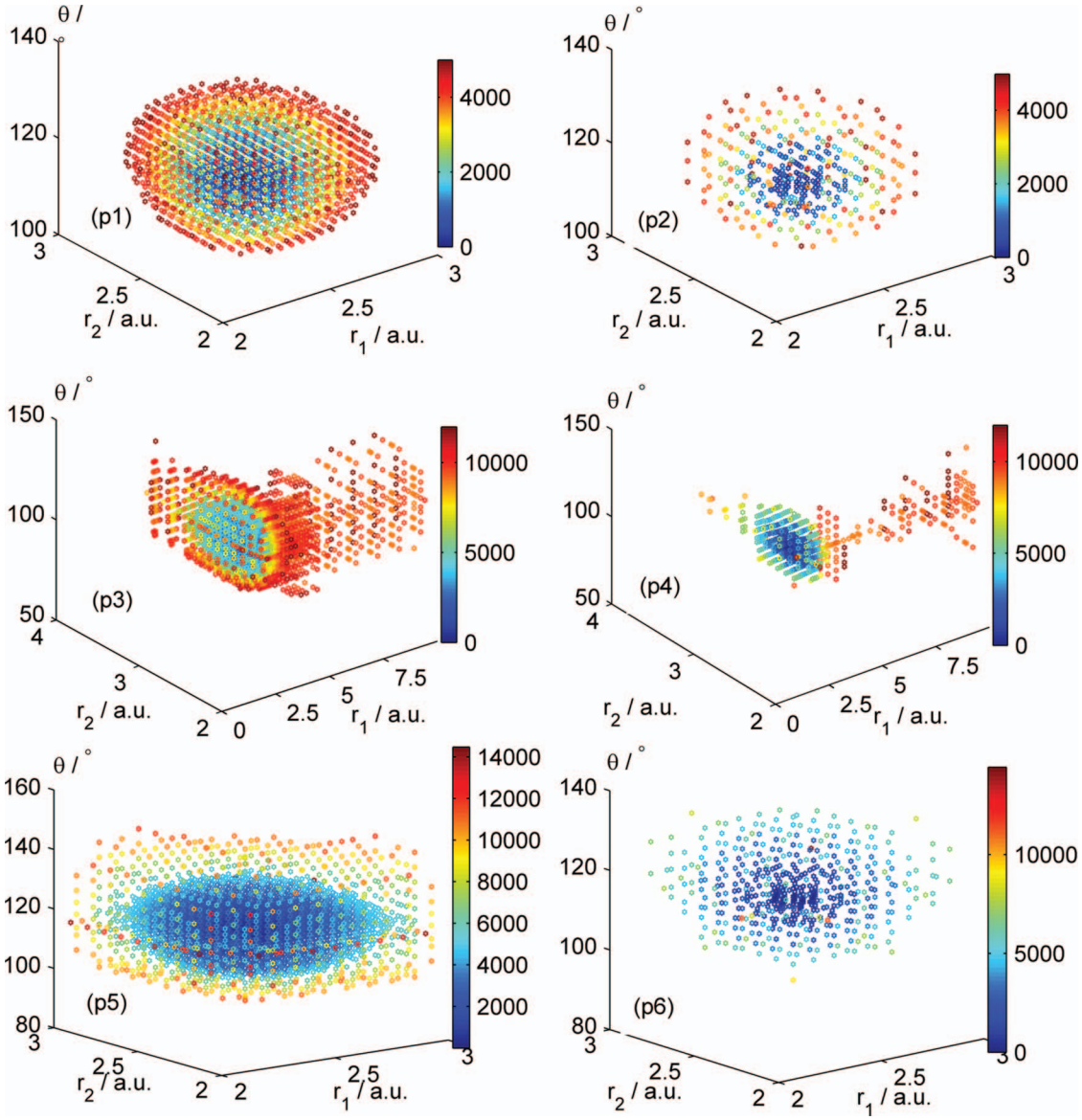

FIG. 1. *Ab initio* electronic ground state energies of the ozone molecule in 4D representation illustrating the grid density of nuclear geometrical configurations for our AV5Z and AV6Z calculations. The calculations are essentially focused on the main potential well and on the way towards the dissociation transition state. Left-hand side corresponds to X = 5 and right-hand side to X = 6 AVXZ calculations. Horizontal axes correspond to bond lengths r_1 and r_2 (in a.u.), vertical axe to the apex angle (in degrees), and the scale of the electronic energy E-E_0 (in cm^{-1}) is given in color.

extrapolated electronic energies obtained by ansatz *a*1 with AVQZ, AV5Z, and AV6Z basis sets on a common grid using the X^{-3} two-point extrapolation formula[84,85] (1). First, the points calculated with the different basis sets, as well as the extrapolated ones were fitted with a standard polynomial PES model in bond lengths-bond angle displacements near the C_{2v} equilibrium configuration, then from the resulting force constants we obtained the forms and harmonic frequencies of the normal mode vibrations using the GF Wilson formalism.[86] The primary fit shows that our *ab initio* values in the main well obtained with ansatz *a*1 fit the surface very smoothly: the root-mean-square (RMS) deviation was only 0.004 cm^{-1} up to E-E_0 < 5300 cm^{-1} with the number of parameters much less (by an order of magnitude) than the number of points. This was not always the case: for other ansätze which we also tested, the scatter of *ab initio* values could result in a much more erratic behaviour. For this reason we have chosen the *a*1 scheme for the spectroscopically accessible range of nuclear configurations where the accuracy requirements are the most important. In order to check the stability of the force constants, we have tested the fits with higher energy cut-off of 7500 cm^{-1} and with two orders of the PES polynomial, o6 and o8. Harmonic vibrational frequencies were very robust with respect to these changes and thus their behaviour with increasing *X* could be reliably established. The corresponding values are given in Table I and plotted in Figures 2(a)–2(c).

The ω_i values for sextulplet-zeta and CBS level of the theory are obtained here for the first time. It is assuring that (Q,5), (Q,6), and (5,6) extrapolations are very close on this scale. The *ab initio* values are compared with the harmonic frequencies of an empirical PES which has been obtained through a simultaneous fit to experimental vibration-rotation energy levels of six ozone isotopic species[38] that was an improvement with respect to the previous work.[87] This PES

TABLE I. Harmonic normal mode frequencies (ω_i), stretching force constant (f_{rr}), TS characteristic points, and dissociation energy calculated for $^{16}O_3$ using ic-MRCI-Q_D/AVXZ with one electronic state optimization.[a]

Basis	AVTZ	AVQZ	AV5Z	AV6Z	CBS(4,5)	CBS(4,6)	CBS(5,6)	Empiric[38]
ω_1	1108.3	1128.8	1133.2	1135.8	1137.8	1138.5	1138.3	1132.1
ω_2	699.7	710.4	712.5	714.2	714.7	715.5	715.9	714.4
ω_3	1053.3	1082.6	1089.4	1093.7	1096.6	1097.7	1097.9	1087.1
f_{rr}	2.8828	3.0142	3.0444	3.0631	3.0760	3.0814	3.0816	3.0407
B ($r_2 = 3.9$)	7927	8599	8807	8897	9025	9023	9021	
vdW ($r_2 = 4.5$)	7858	8567	8779	8873	9002	9001	9001	
D ($r_2 = 12$)	8029	8739	8936	9028	9143	9150	9155	

[a]Standard spectroscopic units are used: the force constant f_{rr} is mdyne × Å^{-1}, all other quantities are in cm^{-1}; B – the reef barrier height, vdW- van der Waals well point, D – dissociation threshold calculated with respect to E_0 on the MEP with θ fixed to 117° at the r_2 value given in a.u.

was the most precise one for rotational calculations as well as for vibrations at low energies resulting in a RMS deviation of 0.02 cm^{-1} for E < 3800 cm^{-1}, and 0.12 cm^{-1} for E < 4500 cm^{-1} above the zero point energy (ZPE) for isotopic data available at that time.

The bending frequency ω_2 has been underestimated in all previous *ab initio* calculations because the bending cut of the PES was too shallow both at cc-pVQZ[21] and AV5Z[33] levels of calculations as already noticed in our previous work.[33] This is also seen in Figure 2: the results indicate though that this issue might be solved if the PES is computed with $X = 6$ or by using CBS extrapolation. On the other hand, the behaviour of stretching frequencies ω_1 and ω_3 looks puzzling as the plots of Figures 2(b) and 2(c) suggest that the quality of vibrational predictions would drastically deteriorate with increasing cardinal number ($X = 6$) and at the CBS limit. The CBS(5,6) extrapolation overestimates ω_3 by ~11 cm^{-1}, consequently the expected error for 7- or 8-quanta bands, which

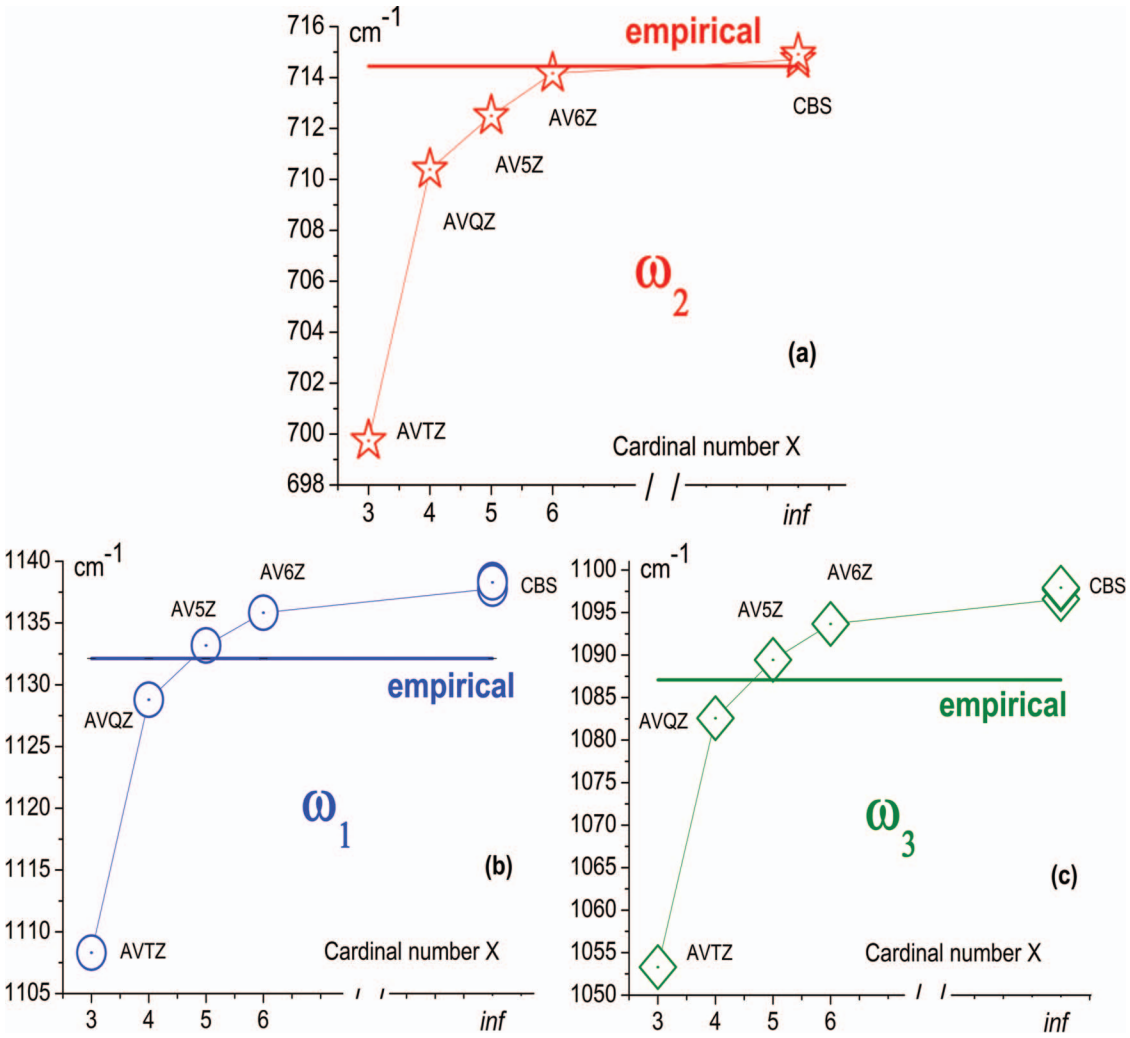

FIG. 2. (a)-(c) Harmonic frequencies versus the cardinal number X of the atomic basis set with the setup of Table I.

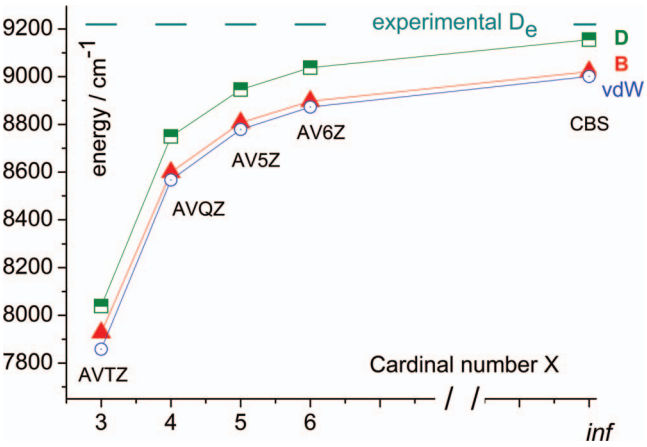

FIG. 3. Barrier (B) of the reef structure, van der Waals well point (vdW), and dissociation threshold (D) versus the cardinal number X. All quantities are calculated with respect to E_0 on the MEP with θ fixed to 117° (Table I).

are currently under study,[16–19] would amount up to about 80 cm^{-1}. This would make such predictions completely useless for high-resolution spectral analyses.

The explanation of this unexpected behaviour of the stretching modes is not trivial. For example, this cannot be explained by missing energy contributions: a qualitative estimation for core-valence contributions accounted for in our previous study[33] gives even higher frequencies; relativistic effects are too small compared to this error; the spin-orbit coupling in the O atom fragment at the dissociation could not significantly affect the vibrational states in the main ozone well; the Born-Oppenheimer breakdown effects are not expected to be that large for this relatively heavy molecule: preliminary estimations of the diagonal Born-Oppenheimer corrections (DBOC) gave the contributions to fundamental vibrations much below one wavenumber. In our opinion, the key to the understanding might be found in the X dependence of three quantities: the ω_1, ω_3 frequencies on the one hand and the f_{rr} force constant (defined as the second PES derivative at the equilibrium with respect to the bond length $f_{rr} = (\partial^2 U/\partial r^2)_e/2$) and the height of the reef barrier (denoted as (B) in Table I and in Figure 3) on the other hand. The dissociation threshold $D(X)$ gradually increases with X approaching the experimental value of 9219 cm^{-1} (Rusic *et al.*[88,89]), the trend being known from all previous studies.[23–33] The absolute value of the reef barrier (measured from the E_0 in the bottom of the C_{2v} well and denoted as (B) in Table I and in Figure 3) remains below the dissociation limit ($B < D$) but increases as well, at least in case of calculations with internally contracted methods and using orbitals obtained for one electronic state only. Note that the plot in Figure 3 for $B(X)$ computed at ic-MRCI/AVXZ level is fully consistent with ic-MRAQCC/CVXZ calculations (Table IV of Ref. 33). The increasing $B(X)$ value causes that the stretching cut of the PES $U(r, r_e, \theta_e)$ becomes more and more tight. This is clearly seen on the behaviour of the stretching force constant $f_{rr}(X)$ in Table I. Consequently $\omega_1(X)$ and $\omega_3(X)$ increase as well becoming much larger than acceptable in case of $X > 5$. This finding suggests that in a PES producing good stretching vibrations the reef barrier should be much lower or even fully vanish.

The existence of the ozone TS barrier has been questioned in many previous *ab initio* works.[9,29,31–33] Let us remind that in earlier studies the TS barrier was considered as a true barrier above D_e, but with improving methods and basis sets it has been found (Hernandez-Lamoneda *et al.*,[29] Siebert *et al.*,[20,21] Fleurat-Lessard *et al.*[32]) that B submerged below D_e. Note that in our calculations with a large CAS(18,12) and with AVXZ basis B was below D_e already with triple (X = T) and quadruple (X = Q) basis. However even this reef barrier prevented one from consistent kinetic calculations. Schinke *et al.*[1] have concluded that only a PES with an artificially removed reef barrier yielded reasonable agreement with experimental rate coefficient. This conclusion is now augmented by our finding that relatively high B value also prevents agreement for vibrational levels. This latter issue has not been evidenced in previous studies because available 3D PESs were calculated with insufficiently large basis sets.

A legitimate question is then: would this reef TS structure survive with improving the electronic structure theory or would it disappear? There are at least two strong arguments in favour of the latter choice. Recently, Dawes *et al.*[9] investigated how the inclusion of several electronic states in the ic-MRCI procedure influences the calculated ground state PES, in particular near TS. They have considered 13 singlet electronic states potentially relevant for the adiabatic dissociation of ozone in the C_s symmetry. Their calculations differed in two ways form earlier calculations. First, in the CASSCF step all 13 states have been included in the state averaging (SA) through dynamic-weighting (DW-CASSCF)[90] resulting in appropriate orbitals for all regions of the PES. Second, in the ic-MRCI procedure the two lowest states of these 13 have been included as reference functions allowing a more proper description of the interacting states at the avoided crossing region. Using this ansatz, they have reported ic-MRCI+Q_D results along the MEP near the TS. These calculations resulted in a monotonically decaying MEP function while shortening the dissociation coordinate and "the disappearance of the 'reef' structure was attributed primarily to including the ten upper states in the DW-SA-CASSCF reference, which smoothes the transition through the region of the avoided crossing."[9] As these calculations are quite demanding, only 2D PES based on AVTZ and AVQZ basis sets along with (T,Q) extrapolation was reported[9] and the discussion was limited to the TS range. After having applied an approximate quantum statistical model, Dawes *et al.*[9] have concluded that the absence of this submerged barrier would have important implications for kinetics bringing rate constants into a much better agreement with experimental data and that exact quantum dynamics calculations would require a full-dimensional PES.

The other hint comes from the calculations of Müller *et al.*:[91] performing non-contracted MRCI calculations they have found that the reef structure could be an artefact of internally contracted ansatz. This is consistent with Dawes' results discussed above since including a second state as reference in the ic-MRCI ansatz its flexibility is increased, the interaction of these two can serve as a proper basis in the avoided crossing region. A non-internally contracted ansatz includes this (and other) interaction by construction. Unfortunately,

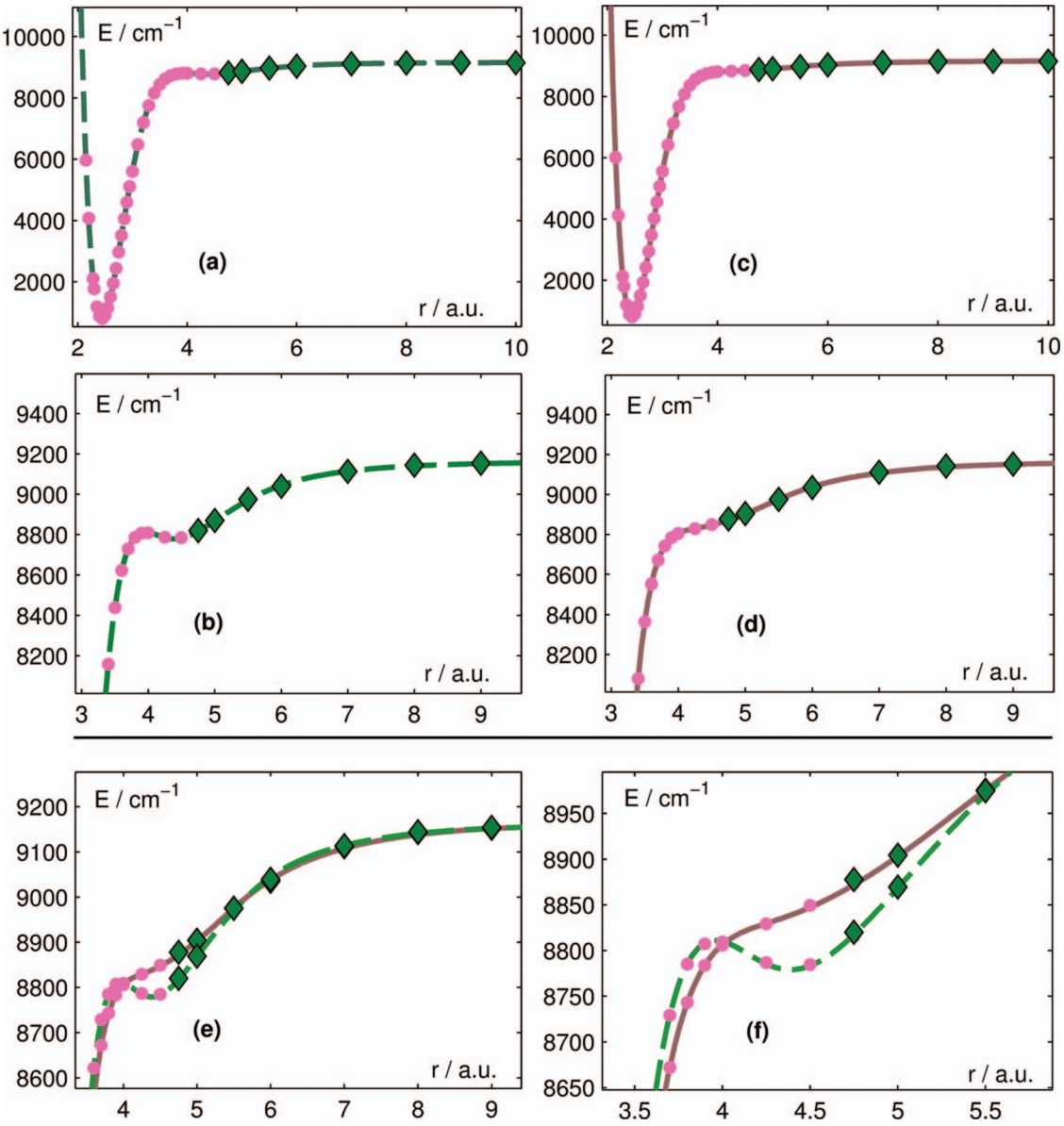

FIG. 4. 1D r_1-cuts of two PES versions with $r_2 = 2.28$ a.u. and $\theta = 117^\circ$. Magenta-dots and green-diamond points refer to icMR-CISD+Q_D *ab initio* calculations with $a1$ and $a5$ ansätze correspondingly; the range $r \sim 4.5$-5.5 a.u. corresponds to $a1/a5$ smoothing (see the text). Panels (a and b): Dashed curve for R_PES with reef structure (one electronic state optimisation). Panels (c and d): Continuous curve for NR_PES without reef structure. The latter is removed using the 1D MEP correction due to Dawes *et al.*[9] accounting for two reference functions in the ic-MRCI calculations along with orbitals from full-valence 13-state DWSA-CASSCF. Panels (e and f): Comparison of R_PES and NR_PES at the TS range. The fit of these two PES versions to *ab initio* points is described in Sec. V.

the non-contracted MRCI calculations are extremely demanding and the results with sufficiently large basis set are not available.

We have decided to build two versions of PES using our best *ab initio* results as discussed in the forthcoming Sec. V. The first one is built with a reasonable value of B keeping the reef structure, which, in what follows, will be referred to as R_PES ("reef PES"). Another one is built by applying 2D stretching correction obtained from Dawes' calculations, which will be referred to as NR_PES ("no reef PES"). A 1D comparison of these two versions of *ab initio* PES along the MEP cut is given in Figures 4(a)–4(f). It is seen that NR_PES has shallower stretching cut. The 3D version of these PESs combining best available *ab initio* results constructed in Secs. IV and V are subsequently used for vibrational predictions and compared with experimental spectroscopic data in Secs. VI and VII.

IV. ANALYTICAL REPRESENTATION OF THE PES: MINIMUM ENERGY PATH MODEL

A 3D spline PES interpolation has well-known advantages and limitations. An obvious advantage is a possibility of representing complicated shapes of global surfaces. However, a reliable 3D spline interpolation requires filling the entire nuclear configuration space by a grid of *ab initio* points even in ranges which are of no use for spectroscopy or for dynamics. Also, this method is very sensitive to outliers due to

possible poorly converged points. A physically justified analytical PES representation should be in a sense more robust. This also allows a more flexible choice of the grid by increasing the density of points in the ranges important for spectroscopy applications as shown in Figure 1.

Various analytical PES representations for triatomic molecules are widely used in the literature: see, for example, Murrell *et al.*,[92] Jensen,[93,94] Partridge and Schwenke,[60,61] Braams and Bowman,[95] and references therein. Some of them were applied to the ozone PES.[36–38,96–98] Carter *et al.*,[96] Varandas *et al.*,[97,98] and Murrell *et al.*[92] introduced empirical corrections to the ozone potential surface to account for scattering and kinetic rate data. Ayouz and Babikov[35] have recently applied permutationally invariant polynomial method[95] to fit ozone PES with a more realistic D_e limit than in the original work of Siebert *et al.*,[20,21] but their vibrational predictions were much less accurate. Up to recently the most accurate vibration-rotation calculations has been provided with empirically fitted (*morse*) × (*cosine*) type analytical PES parameterization[36–38] which had been used for analyses of experimental spectra[13–19] and for the predictions of methastable doorway states.[18] This latter representation gave quite accurate band centers[13,15,19] up to 7000 cm^{-1} with an average error of ∼1 cm^{-1}, but extrapolation to higher energies were less reliable[16,19] presumably because this analytical form was not flexible enough for describing the shape of the PES at large internuclear distances.

As already mentioned in the Introduction the shape of the ozone PES is particularly complicated. In addition to the specific features in the bottleneck TS range discussed in Refs. 9, 20, 21, and 31–33 and in Sec. III, the ozone PES has some more peculiarities. Here we mention one which is not necessarily exclusive feature of ozone, but absolutely necessary to consider to obtain a correct PES. Contrary to the case of many other triatomics like water molecule, the ozone PES does not have an additivity property with respect to the molecular fragmentation: in order to break one bond, one needs about 1 eV and of course the same energy to break another bond, but for breaking both bonds one needs more than 5 eV. This is because the molecular oxygen O_2 has much more profound potential well than the ozone molecule, i.e., the bond in O_2 is much stronger than the one in ozone. This means that there is a great deal of rearrangement of electron pairs what requires multireference description. As a result r_e (O–O) value is shrinking down from 2.4 a.u. (ozone) to 2.28 a.u. (diatomic oxygen) when one oxygen atom is taken off. Therefore, the ozone MEP is significantly nonlinear near the C_{2V} open structure (nuclear equilibrium configuration) and cannot be modeled by a standard Morse approximation for the "plane" O–O stretching PES cut; the latter would overestimate the dissociation energy by about 950 cm^{-1} that represents a huge error. Consequently, for example, the PES model of Partridge and Schwenke,[60] which was very successful for the water molecule, would not be directly applicable for the ozone without appropriate modifications.

In this work we propose a new analytical model for the ozone PES which aims at accounting for the above-mentioned features. This representation is limited to the range which is essential for spectroscopy and dynamics applications: in the vicinity of the main open structure equilibrium and along the minimum energy path towards the dissociation. As was argued in Ref. 36, in order to relate the global potential surface with such an effective potential function, it is convenient to divide the entire vibrational coordinate space r_1, r_2, r_3 into three sectors:

$$(s1): r_2 < r_1; r_3 < r_1 \qquad (s2): r_1 < r_2; r_3 < r_2$$
$$(s3): r_1 < r_3; r_2 < r_3. \tag{2}$$

Here r_1, r_2, and r_3 are internuclear distances. The sectors ($s1$), ($s2$), and ($s3$) each have an open structure minimum and all three minima are equivalent. It is clear that it is sufficient to know the potential function within only one of the sectors. An extension to the other sectors can be made by symmetry operations permuting the central nucleus to an "end" position. In the present work, we assume that the potential energy barriers between different C_{2V} minima, and between each C_{2V} minimum and the possible metastable ring structure minimum with $r_1 = r_2 = r_3$, are sufficiently high to be insuperable on the time scale of the experiments with which we are concerned. This assumption is supported by previous global *ab initio* PES calculations[20,21,23] and by the fact that all available experimental data can be interpreted in terms of asymmetric top effective Hamiltonians which is consistent with one C_{2V} structure for the molecule. We disregard here a ring ozone structure[22,23] which should not be relevant to spectroscopic and dynamic studies of ozone in gas phase under presently accessible experimental conditions.

Our analytical representation in the ($s3$) sector of the nuclear configuration space is built in several steps and can be schematically written as follows:

$$U(r_1, r_2, \theta) = S(r_1, r_2) + h(r_1, r_2) + P_n(r_1, r_2, \theta)G(r_1, r_2) + P^{(a)}(\theta)G^{(a)}(r_1, r_2), \tag{3}$$

where the $S(r_1, r_2)$ and $h(r_1, r_2)$ functions represent the stretching "skeleton" of the PES in the considered range. The first term

$$S(r_1, r_2) = \sum_{i \geq j,\ i+j>1} K_{ij}\left(y_1^i y_2^j + y_1^j y_2^i\right) \tag{4}$$

is an expansion in modified curvilinear Morse-type y-functions. Contrary to a usual Morse-type expansion form[93,60] our y-functions are not "plane"

$$y_1 = 1 - \exp(-a(r_1 - \mu(r_2))), \tag{5a}$$

$$y_2 = 1 - \exp(-a(r_2 - \mu(r_1))), \tag{5b}$$

and depend both on $r_1 = \tilde{O} - O_1$ and $r_2 = \tilde{O} - O_2$ distances, where $\tilde{O}$ denotes the central oxygen atom of the $O_1\tilde{O}O_2$ molecule in the ($s3$) sector. Let r_0 be an initial guess for the equilibrium length of r_1 and r_2 bonds of the open ozone structure: r_0 (O_3) ∼ 2.409 a.u. The $\mu(r)$ function in Eqs. (5a) and (5b) satisfies the following conditions:

$$\mu(r_0) = r_0, \quad \mu(r \to \infty) = d_{mep}, \tag{6}$$

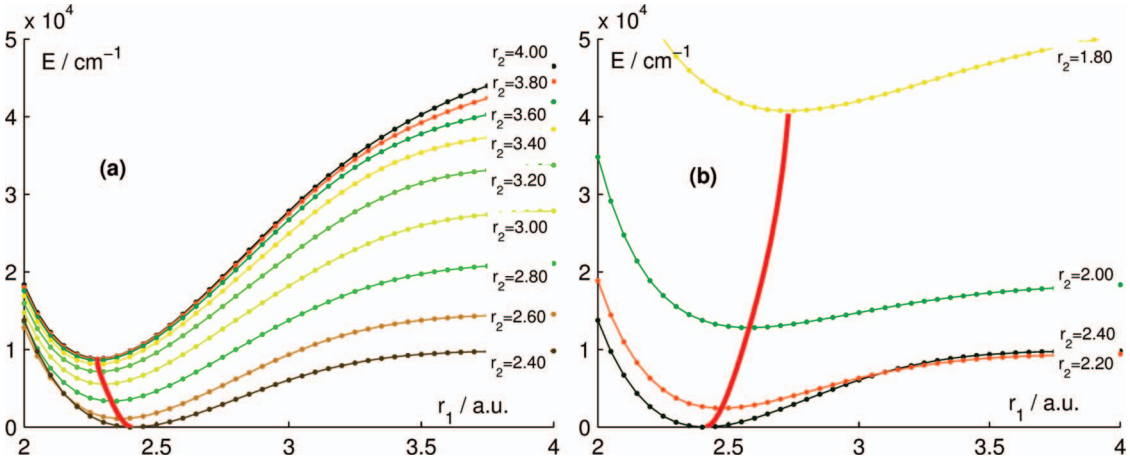

FIG. 5. Non-symmetrized MEP as obtained by simple "drag" method with one bond length successively fixed step-by-step and with another bond relaxed in order to minimise the potential energy. Bond lengths are given in a.u. and energy on the vertical scale in cm^{-1}. Red curve corresponds to the function $r_2^{min} = \mu(r_1)$.

where d_{mep} is the limiting value of equilibrium bond length of the diatomic $O_2(^3\Sigma_g^-)$ fragment at the end of the minimum energy path: $r_e(O_2) = d_{mep} \simeq 2.28$ a.u. There exist various sophisticated algorithms[99–101] for a numerical MEP determination on a given PES. Our aim here is different: we are looking for an analytical approximation $S(r_1, r_2)$ having qualitatively correct asymptotics, the fine tuning of the surface shape will be accounted for by other terms of Eq. (3). For this purpose we proceed in two steps. At the first step the $r_2^{min} = \mu(r_1)$ function is evaluated by a simple "drag" MEP method[99] along the bond length coordinate r_1 in the r_1/r_2 plane: for every fixed r_1 value the PES cuts along r_2 were minimised as illustrated in Figure 5. In our model the corresponding non-symmetrized path is approximated by the following function

$$\mu(r) = (r_0 - d_{mep})(1 - \tanh(g_{mep}(r - r_0))) + d_{mep}, \qquad (7)$$

which accounts for the shrinking of the bond length (d_{mep}) of the O–O diatomic fragment on the way to the dissociation. The g_{mep} parameter defines the slop of the MEP curve in the equilibrium. This function satisfies conditions (6) but does not coincide with a true MEP for $r < r_0$ (dashed curve in Figure 6). This is not a problem because in the $r < r_0$ range the bond length is no more a dissociation coordinates and also because at the second step the symmetrisation in Eq. (4) provides a physically correct MEP (solid curve in Figure 6) for the $S(r_1, r_2)$ surface invariant under the $r_1 \rightleftarrows r_2$ permutation.

In order to illustrate this property let us compare the model ((4)-(7)) with a standard 2D Morse type stretching expansion. The usual 1D Morse oscillator potential $U^{Morse}(r) = D_e\, y^2(r)$ is conveniently expressed via the standard exponential function $y(r) = 1 - \exp(-a(r - r_0))$. The 2D Morse oscillator $U^{Morse}(r_1, r_2) = D_e(y^2(r_1) + y^2(r_2))$ would have an additive property $\min\{U(r_1 \to \infty, r_2)\} + \min\{U(r_1, r_2 \to \infty)\} = U(r_1 \to \infty, r_2 \to \infty)$ with respect to one-particle and two-particles fragmentations which is not the case of the ozone molecule. To account for this non-additivity

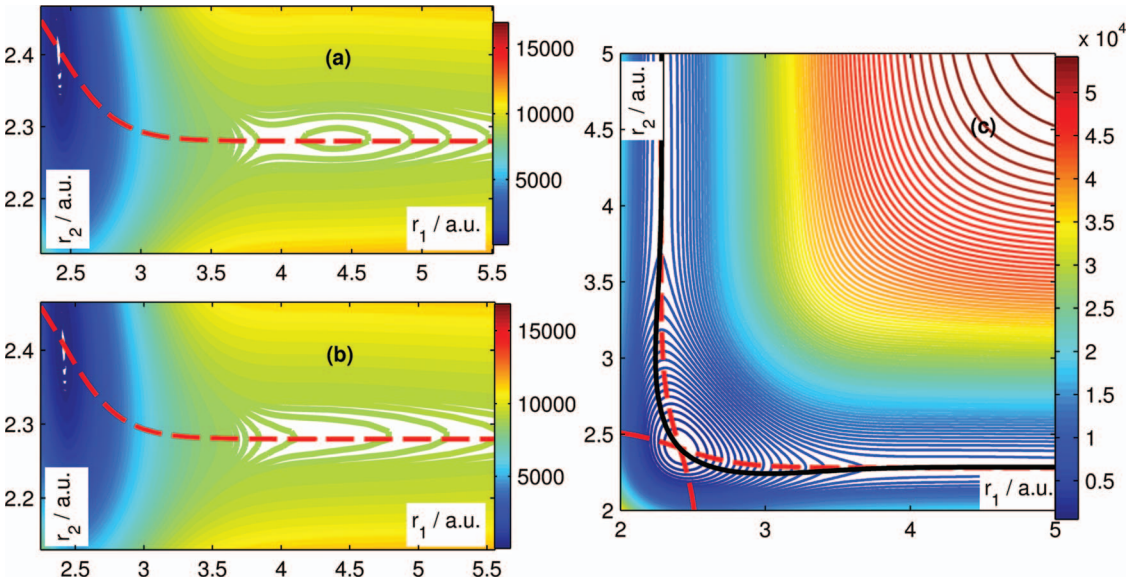

FIG. 6. 2D representation of the non-symmetrized μ-path (red dashed curves) superposed with the contour plots for two versions of the potential: (panel (a)) for the R_PES and (panel (b)) for the NR_PES. (Panel (c)) The symmetrized MEP (solid black curve) for the NR_PES.

property, the products of $y(r_1)$ and $y(r_2)$functions could be added to cast the model in the form (4). Let us consider a simple case of Eq. (4) where all i, j powers are even, $K_{ij} > 0$ and y_1 and y_2 are replaced by the standard Morse 1D functions. Such a model would have the 2D minimum in (r_0, r_0) but in the dissociation channels the PES cuts orthogonal to the dissociation coordinate r_1 would also have a minimum at $r_2 = r_0$. This is not correct for the ozone PES. In the same conditions the model ((4)-(7)) has the 2D minimum in (r_0, r_0) whereas the minima in the dissociation channels are equal to d_{mep}, which can be adjusted to the minimum of the diatomic $O_2(^3\Sigma_g^-)$ fragment. The stretching MEP is thus qualitatively correct and symmetric under the $r_1 \rightleftarrows r_2$ permutation.

The term $h(r_1, r_2)$ in the model (3) is a double-hump stretching function

$$h(r_1, r_2) = C^{(o)} h^{outer}(d^*(r_1, r_2), d_0^*, q^*) + C^{(i)} h^{inner}(d_*(r_1, r_2), d_{0*}, q_*) - h_0, \quad (8)$$

which is designed to account for an eventual reef structure at the TS path or for flat PES regions where the convexity of the surface could change. The constant h_0 is chosen in a way to keep the 2D equilibrium (r_0, r_0) of the first PES term $S(r_1, r_2)$ unaltered. Function (8) has a stationary point in (r_0, r_0) that determines the value of the $C^{(i)}$ constant. Both inner and outer humps have the same Gaussian radial form

$$h^{outer/inner}(d(r_1, r_2), d_0, q) = \exp\left(-4.5\left(\frac{d(r_1, r_2) - d_0}{q}\right)^2\right), \quad (9)$$

where d_0 and q are parameters, while $d(r_1, r_2) = (r_1)^4 + (r_2)^4$ is the distance measure between (r_1, r_2) and the origin $(r_1 = 0, r_2 = 0)$.

The bending part of the PES, as well as bend-stretch and stretch-stretch corrections are described by last two terms in Eq. (3). The third part is a polynomial in bond displacements and cosines of angles

$$P_n(r_1, r_2, \theta) = \sum_{\substack{i,j,k,\\ i\geq j,\\ i+j+k\leq n,}} C_{ijk}\left(\left(\frac{r_1 - r_0}{r_0}\right)^i\left(\frac{r_2 - r_0}{r_0}\right)^j + \left(\frac{r_1 - r_0}{r_0}\right)^j\left(\frac{r_2 - r_0}{r_0}\right)^i\right)(\cos(\theta) - \cos(\theta_0))^k \quad (10)$$

multiplied by a damping Gaussian function

$$G(r_1, r_2) = \exp(-g_s((r_1 - r_0)^2 + (r_2 - r_0)^2) - g_{ss}((r_1 - r_0)^2(r_2 - r_0)^2)). \quad (11)$$

This factor suppresses a non-physical behavior of a polynomial at large internuclear distances in a way that PES asymptotes are determined by the $S(r_1, r_2)$ term. Equations (10) and (11) are similar to those used by Partridge and Schwenke[60] except for the last term in Eq. (11) which helps to emphasize or de-emphasize the damping along the symmetric stretch coordinate. Finally, we added an angular term

$$P^{(a)}(\theta) = \sum_{k=0} C_k^{(a)} (\cos(\theta) - \cos(\theta_0))^k \quad (12)$$

multiplied by the damping factor $G^{(a)}(r_1, r_2)$ which has the same form as Eq. (11) but with different parameters $g_s^{(a)}$ and $g_{ss}^{(a)}$. A combination of these differently damped terms is useful because the angular PES dependence is quite different in the bottom of the C_{2V} well and at large distances.

V. FIT OF THE SURFACES TO *AB INITIO* POINTS

As already stated in Sec. III we constructed in this work two versions of the ozone ground electronic state PES by combining best available *ab initio* calculations: one with the "reef" structure on the TS path (R_PES) and another one without the reef feature by accounting for Dawes 2D corrections (NR_PES). Appropriate sets of points and corrections were used for these purposes. In the spectroscopically accessible range up to the TS ($r < 4.5$ a.u.) the most accurate 3D calculation were obtained with the ansatz $a1$ as explained in Secs. II and III. On the way to the dissociation this was completed by a grid of points computed with $a5$ ansatz providing more stable convergence at large distances. In the boundary regions we have computed points with both ansätze. This allowed us smoothing the surface by matching $a5$ calculations continuously to more accurate $a1$ values (for example, at the reef barrier the shift was only 4 cm^{-1} between 8807 cm^{-1} ($a1$) and 8811 cm^{-1} ($a5$) at $r_1 = 2.28$ a.u., $r_2 = 3.9$ a.u., and A = 117° with AV5Z basis set). Once again this $a5/a1$ smoothing which occurs at large distances does not have any effect on spectroscopically observed bands.

For the R_PES we start by using ic-MRCI_AV5Z_a1 *ab initio* values in the main potential well. This is because X = 5 calculations are the most representative (1950 points) and because stretching harmonic frequencies $\omega_1(X = 5)$ and ω_3 $(X = 5)$ are the closest ones to the empirical values (Figure 2, Table I). In order to provide a more realistic dissociation limit for the surface we have proceeded by the CBS(5,6) extrapolation of $a5$ points beyond the TS range ($r > 5.5$ a.u.) with a smoothing interval ($4.5 < r < 5.5$ a.u.). This procedure does not modify the reef with the submerged barrier on the MEP at $r = 3.9$ a.u. followed by the vdW minimum at $r \sim 4.5$ a.u. and gives the limit $D_e = 9164$ cm^{-1} (evaluated at $r = 12$ a.u.) which is to be compared with experimental determinations $D_e^{obs} = 26.1$ kkal/mol $\Leftrightarrow$ 9129 cm^{-1} (Chase *et al.*[102] value as cited in Refs. 23, 27, and 28) and $D_e^{obs} = 9219$ cm^{-1} (Ruscic[89] value as cited in Ref. 33). The MEP cut of this PES is shown in Figures 4(a)–4(f) with the reef structure clearly visible: $a1$ *ab initio* points in red dots and $a5$ points in green diamonds.

If we proceed with the CBS(5,6) point-by-point extrapolations in the spectroscopically accessible range the stretching vibrational levels would be very much overestimated as follows from Figures 2(a) and 2(b). For this reason at the first step of the R_PES construction we did not do the extrapolation in this way. This hybrid sample of *ab initio* points was used to fit the parameters of the R_PES using the model described in Sec. IV. The RMS deviations of the fit are given in

TABLE II. Root-mean-square deviations of the PES fit to *ab initio* points using the analytical model ((3)-(12)) versus the energy cut-off E_{max}.[a]

E_{max}	R_PES RMS	NR_PES RMS	E_{max}	R_PES r ≤ 4.5 RMS	R_PES r ≤ 10 RMS	NR_PES r ≤ 4.5 RMS	NR_PES r ≤ 10 RMS
3000	0.038	0.037	9200(*)	0.55	1.31	0.51	1.00
5000	0.079	0.082	9650(#)	0.63	3.94	0.60	2.68
8000	0.161	0.170	10000(§)	0.75	5.25	0.72	3.52

[a]The values for E_{max} and for RMS deviations are given in cm^{-1}. Limitations for internuclear distance r are in a.u.: the range (r ≤ 4.5 a.u.) corresponds to currently accessible spectroscopic high-resolution experiments. (*) energy range just above the PES dissociation limit; (#) energy range corresponding to room temperature and low temperature dynamics; (§) energy range corresponding to high temperature dynamics.

Table II and the scatter of (*ab initio – fitted*) points is shown in Figures 7(a)–7(d).

In order to build the NR_PES we applied to our best *ab initio* 3D PES the 2D stretching corrections which are due to the improved method of calculations in the TS range described by Dawes *et al.*[9]

Initially, for the reasons explained above, we started with the same sample of *a*1/*a*5 points using very dense and representative grid of ic-MRCI_AV5Z values. The Dawes MEP cut has been computed at the ic-MRCI_AVTZ and ic-MRCI_AVQZ levels but with subsequent CBS(T,Q) extrapolations. For the consistency with this data we also made, as a first step, the stretching CBS extrapolation on the same MEP though at the CBS(5,6) level. This gave the reef barrier height of 9022 cm^{-1} at $r_1 = 3.9$ a.u. and $r_2 = 2.28$ a.u. and consequently too high $\omega_1(CBS)$ and $\omega_3(CBS)$. Then in a similar way we applied Dawes correction calculated as the difference between our initial PES and the Dawes result on the 1D MEP with subsequent symmetrisation $r_1 \rightleftarrows r_2$ leading to a simple 2D stretching correction

$$Corr^{2D}(r_1, r_2) = Corr^{1D}(r_1, r_2^*) + Corr^{1D}(r_1^*, r_2) \quad (13)$$

which were interpolated to the equilibrium bond length. Here r_i^* corresponds to the optimized value (d_{mep}) of the diatomic bond length on the MEP. The resulting points were fitted with the 3D surface model ((3)-(12)), the RMS deviations being given in Figures 7(a)–7(d) and in Table II. With this latter contribution (13) the reef barrier disappears, the corresponding MEP curve being shown in the right-hand side panels of Figure 4.

As shown in Sec. III, with the AV5Z basis the bending harmonic frequency ω_2 was underestimated. To improve bending vibration levels we applied the CBS(5,6) extrapolation for the principle PES bending parameter C_{002} as follows. This quadratic angular parameter in Eq. (10) was shifted by a correction $\Delta C_{002} = 319.17$ in a way that

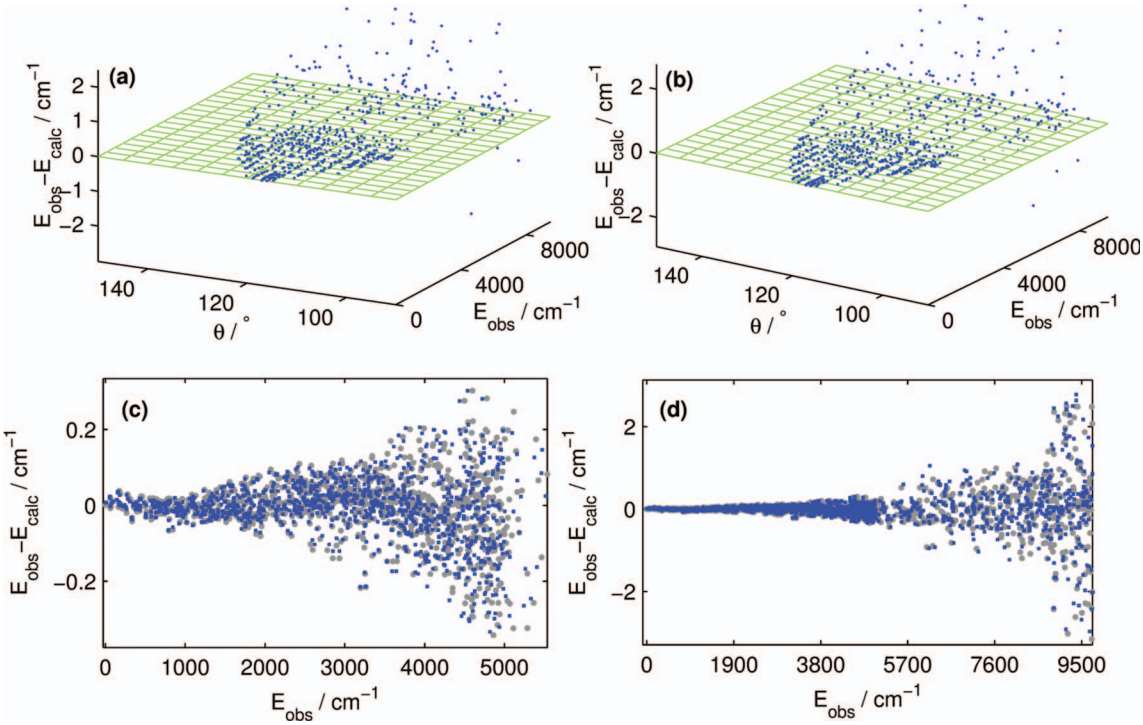

FIG. 7. Scatter of *ab initio* points fitted with the MEP analytical model for two versions of the PES. Fit residuals are given in vertical scale for the R_PES (panel (a)) and for the NR_PES (panel (b)) in the 2D representation versus the apex $O - \tilde{O} - O$ angle (from 90° to 145°) and versus increasing energy up to 9200 cm^{-1}. Panels (c) and (d): the fit residuals shown in blue (R_PES) and gray (NR_PES) cycles are plotted for two regions: main C_{2V} well (E-E_0 < 5000 cm^{-1}) and up to "dynamical" range above the dissociation (E-E_0 < 9500 cm^{-1}).

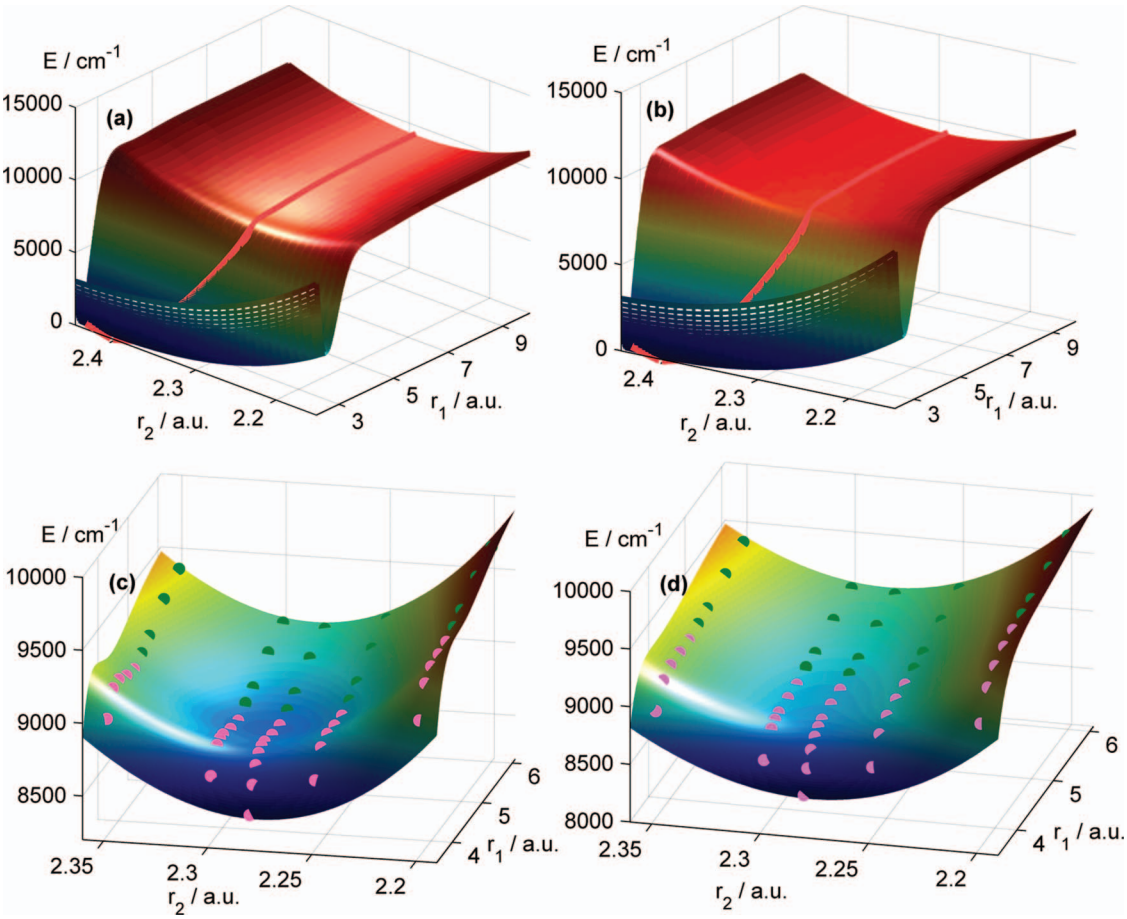

FIG. 8. The stretch-stretch cut of the ozone ground electronic transition state range towards the dissociation for two versions of PES: left-side panels (a), (c): for R_PES and right-side panels (b), (d) for NR_PES. The MEP on the overall view from the C_{2V} equilibrium up to D_e is shown in red on the upper panels. The blown up scale of the lower panels gives a comparison of the analytical surfaces with *ab initio* energies: (*a*1) calculations for red points and (*a*5) calculations for green points. The apex angle if fixed to 117° (near equilibrium value). The bond lengths r_1 and r_2 are given in a.u. and the PES values in cm^{-1} on the vertical scale.

$\omega_2 \rightarrow \omega_2(CBS(5,6))$. This provides a very small "contraction" of the bending PES cut in the main potential well. Indeed, by fitting AV5Z points in this range up to 5500 cm^{-1} with a simple polynomial (10) we obtain $C_{002} = 33431.72$. Thus a relative CBS bending correction is only $\Delta C_{002}/C_{002} = 0.0095$ that is less than 1%. This approach is much simpler than a point-by-points extrapolation and also gives better statistically determined PES parameters because $N_{points}/N_{parameters} \sim 10$ for the dense grid of AV5Z calculations, whereas this ratio would be considerably lower for expensive AV6Z points (see Figure 1).

The comparison of two surfaces near the TS range is given in Figures 8(a)–8(d) which also shows the MEP and the surface agreement with *ab initio* electronic energies. The reef structure (submerged barrier followed by vdW shallow well) is clearly seen at the left-hand panels 8(a), 8(c) for the R_PES, whereas the NR_PES does not show these features.

The projections of the PESs on the r_1/r_2 plane and on the r/θ plane including the corresponding grids of *ab initio* points and contour plots (distinguished by colours indicated at the right-hand scale) are given in Figure 9.

The shape of the analytical PES representation for the stretch-bend cut in the main C_{2V} well and for larger internuclear distances up to 6 a.u. is given in Figure 10, which also shows a very good agreement with *ab initio* values. Finally, the global stretching NR_PES shape for $\theta = 117°$ in the (s3) sector is illustrated in Figure 11, which shows both the main C_{2V} well, dissociation channels along the MES, corresponding to O_2 equilibrium distance ~2.28 a.u., and also asymptotic range with large r_1 and r_2 bond lengths. Figures 9–12 give a bird's-eye view on the surfaces; the distinctions between two versions of the PES are not visible on this scale.

In order to assure a physically correct PES behaviour beyond the main well and beyond the dissociation channels we have also included in the fit additional points obtained from SSB spline PES[20,21] by appropriate energy shifts. These auxiliary "outer" points shown with gray cycles in Figures 9 and 11 correspond to energies higher than 14 000 cm^{-1} much above D_e. They were included in the fit with very low weight ~0.001 with respect to our *ab initio* calculations and thus do not affect the shape of the PES in the ranges important for spectroscopy and dynamics. The energy shifts for these outer points were obtained by matching the SSB spline PES to our *ab initio* values in the range 8000–15000 cm^{-1} in order to assure a smooth PES shaping at higher energies. As our potential well is more profound than that of SSB,[20,21] these

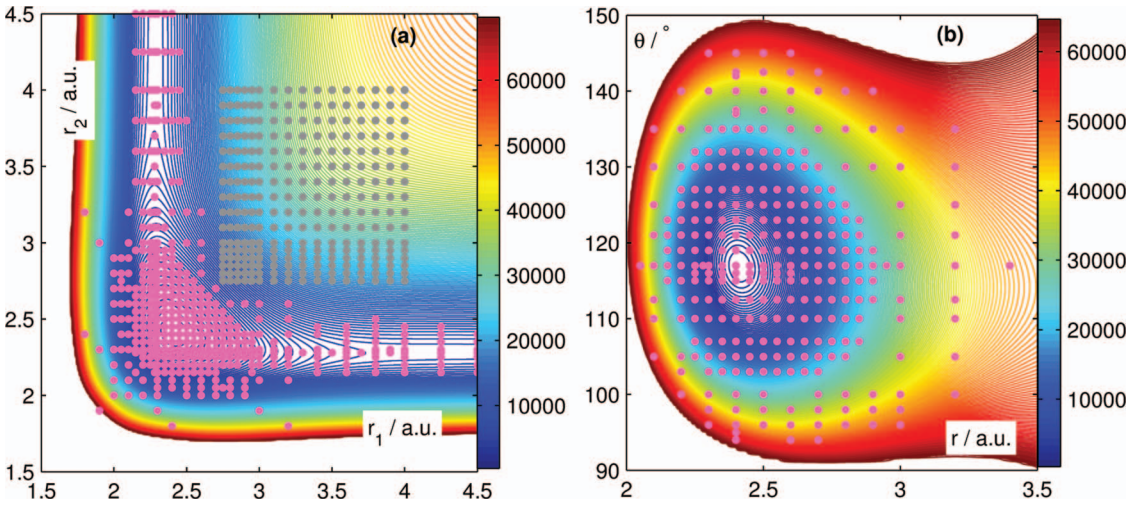

FIG. 9. Stretch-stretch cut (for $\theta = 117^\circ$) and stretch-bend cut (for $r_2 = 2.4$ a.u.) of the NR_PES and sample grids of *ab initio* configurations used in the fit.

auxiliary points were pushed up in average by 800–2000 cm^{-1}. Care has been taken to keep the PES "hole"-free during the fit that is to reject parameter variations which would cause the creation of spurious minima. This was done using the "flexible constraint" approach described in the previous works[36,37] which allows one preventing the formation of spurious minima in the ranges of very small distances or small angles were *ab initio* points were sparse or absent.

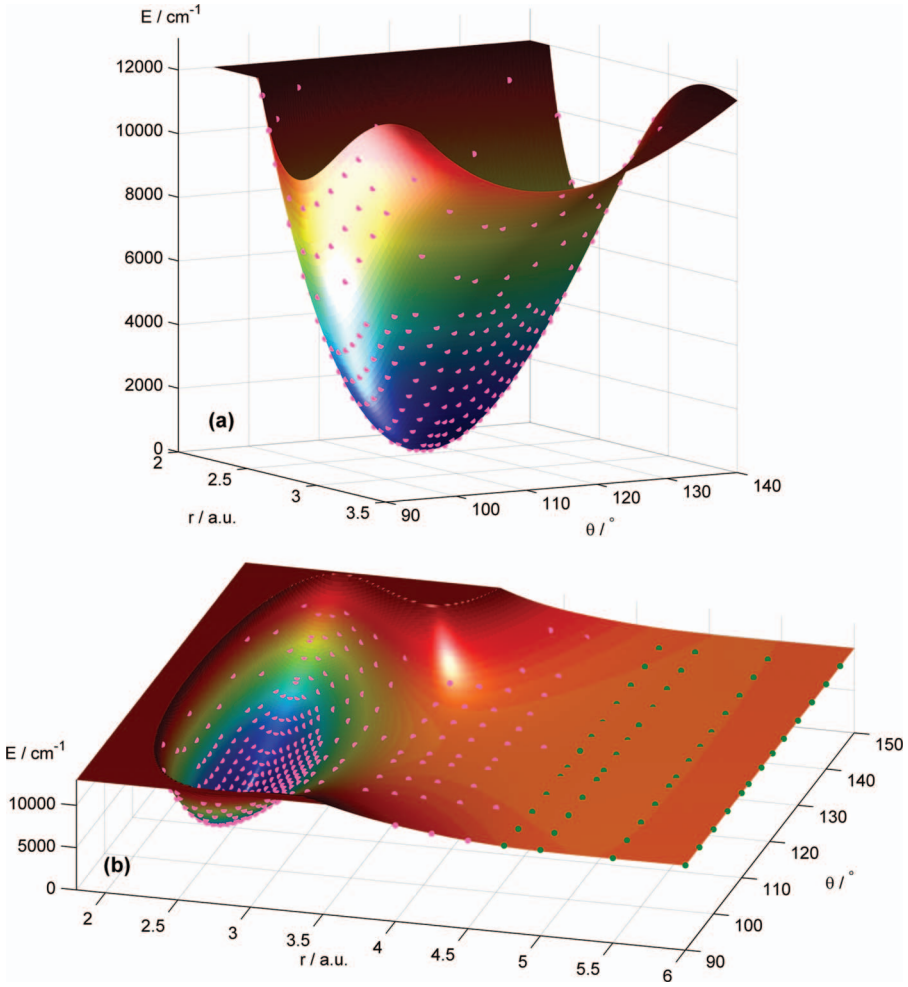

FIG. 10. Comparison of the analytical NR_PES with *ab initio* points for the stretch-bend cut (one bond fixed to the equilibrium value 2.4 a.u.): (a) in the main C_{2V} well; (b) on the way from the main well towards the dissociation. *Ab initio* calculations using $a1$ ansatz are denoted in magenta and those using $a5$ ansatz for $r > 4.5$ in green.

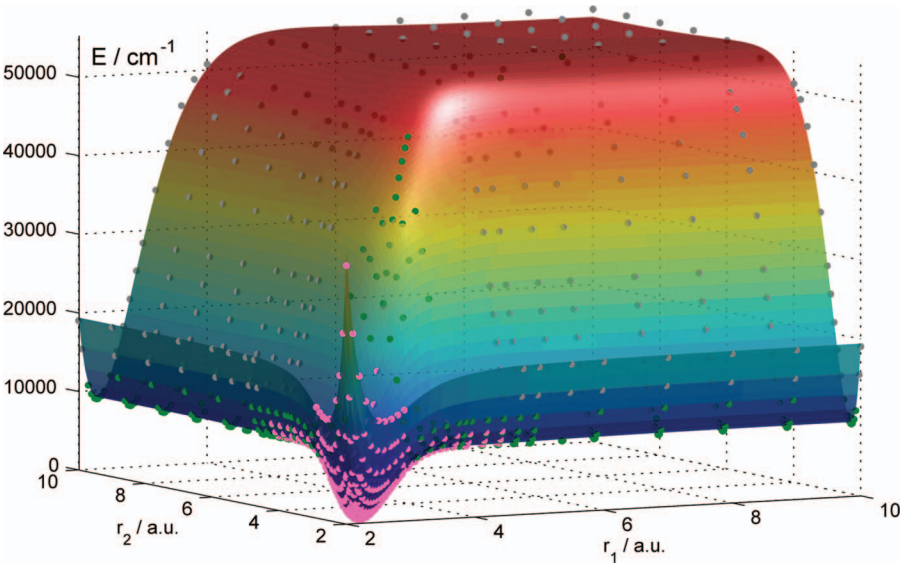

FIG. 11. Global shape of the NR_PES with *ab initio* points: stretch-stretch cut for A = 117° in the main well, in the dissociation $O\tilde{O} - O$ and $O - \tilde{O}O$ channels and for the bisector range towards $O - O - O$ fragmentation. *Ab initio* calculations using *a*1 ansatz are denoted in magenta and those using *a*5 ansatz for $r > 4.5$ in green.

Note that r_0 and θ_0 parameters involved in Eqs. (3)–(11) do not exactly coincide with the C_{2V} equilibrium geometry (r_e, θ_e) if linear terms C_{100} and C_{001} of Eq. (10) are included in the PES fit. Our *ab initio* equilibrium geometry for the NR_PES is $r_e = 2.4095$ a.u. and $\theta_e = 116.78°$ which agree well with empirically determined values $r_e = 2.4052$ a.u. and $\theta_e = 116.75°$ of Refs. 36 and 37. All the PES values quoted in Table I and in text were given with respect to the energy $E_0 = U(r_1 = r_2 = 2.4$ a.u., $\theta = 117°)$ of the reference nuclear configuration which is the closest geometry to the exact equilibrium among the grid points. The PES value $U(r_e, r_e, \theta_e)$ in the exact equilibrium configuration is below the reference E_0 grid value by 9.77 cm^{-1}. Consequently, our CBS(5,6) dissociation limit is $D_e = 9165$ cm^{-1}. The parameters of both surfaces, R_PES and NR_PES, are given in the supplementary material (Appendices A1 and A2).

VI. VARIATIONAL AND DVR CALCULATIONS FOR NUCLEAR MOTION BOUND STATES

There exist various implementations of global methods of calculations of nuclear motion bound states which are particularly important for applications in molecular spectroscopy. A common feature is a numerical solution of the quantum mechanical eigenvalue problem for the nuclear motion Hamiltonian depending on $3N - 3$ suitably chosen

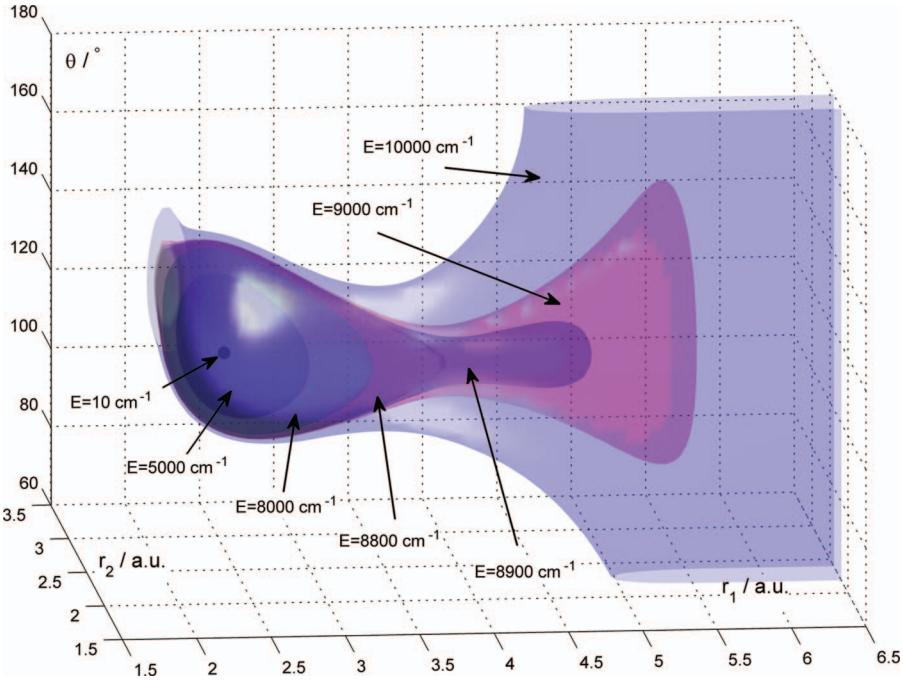

FIG. 12. 4D representation of the global shape of the NR_PES.

rovibrational coordinates. A variational approach (see Refs. 60–75, and references therein) with basis optimization and matrix truncation-compression technique is usually applied. A discrete variable representation (DVR)[103–106] and filter-digitalization[107,108] techniques aimed at improvement of a basis convergence for high-energy range are also widely used. Global methods offer complementary possibilities as compared to traditional band-by-band or polyad-by-polyad effective Hamiltonian models.

In order to compute vibration-rotation energies with the exact kinetic energy (EKE) Hamiltonian, we use the methods and computer codes in the same way as described in previous papers on global calculations for the ozone molecule (see Refs. 36–38 for more details). In order to confirm the results by two independent EKE-methods, we have performed calculations both with the DVR and variational methods which we were able to converge to nearly the same values at least up to 7500 cm^{-1} above the zero-point energy. After having checked the convergence of calculations with three nuclear motion basis sets up to the matrix dimension of the secular problem 17000*17000 in the DVR calculation we estimated that vibrational levels were converged to 0.01 cm^{-1} or better for E < 5000 cm^{-1} and to 0.1 cm^{-1} or better for E < 8000 cm^{-1}.

VII. VIBRATION BAND CENTRES PREDICTIONS AND COMPARISON WITH EXPERIMENTAL DATA

It is well known[55] that for C_{2V} ozone species containing ^{16}O oxygen isotope only rovibrational states of A_1 and A_2 symmetry types are allowed by nuclear spin statistics. Here we use the standard definitions of molecular axes for the I^r representation and the symmetry operations of C_{2V} point group traditionally adopted in ozone spectroscopy:[55] A_1, A_2 irreducible representations being symmetric with respect to C_2 axis and A_2 being anti-symmetric with respect to the molecular plane. Consequently the nuclear spin statistical weight is zero for $J = 0$ levels of B_1-type vibration states of $^{16}O_3$. However, in experimental spectra analyses a centre of the corresponding symmetry allowed rovibrational band is traditionally reported in the literature[13–19,110–140] and defined as $J \to 0$ limit of rovibrational upper state levels. This limit could be experimentally determined from spectra by following transition series in P, Q or R branches in a sufficiently large range of J, K_a values.

For this reason it is instructive to calculate theoretical values for the band centres. The values for the centres of bands $(N' = 0, A_1) \to (N, \Gamma)$ computed with exact kinetic energy operator and the DVR method using our *ab initio* NR_PES are summarised in Table III. Here N' and N are global vibration ranking numbers for the low and upper states according to increasing energy, Γ is a vibration symmetry type of the upper vibrations state and $(N' = 0, A_1)$ stands for the ground vibration state.

Predictions with NR_PES are in excellent agreement (Table IV) with all experimentally available $^{16}O_3$ band centers which have been obtained up to now from analyses of high-resolution ozone spectra.[13–19,110–140] For each observed band we give in Table IV *ab initio* band centres calculated with nuclear (m_{nuc} (^{16}O) = 29148.9455997 m_e) and atomic masses (m_{at} (^{16}O) = 29156.9455997 m_e). Nuclear mass calculations give smaller (*Obs.-Calc.*) deviations for low energy vibrations and atomic mass give somewhat better agreement in higher energy range. The RMS deviations are nearly the same in both cases: 0.99 cm^{-1} for atomic masses and 0.98 cm^{-1} for nuclear masses.

Though ozone, as an asymmetric top molecule in the main potential well, does not have symmetry forbidden rovibrational bands, many transitions in high wavenumber ranges remain too weak to be observed or assigned in current absorption spectroscopy experiments. However, some limited information on the corresponding band centres could be implicitly deduced from spectra analyses via analyses of resonance perturbations of observed transitions (Barbe *et al.*[14–19,118–139]). Upper vibration states for such perturbers are usually called "dark" states. Some other bands (corresponding mostly to symmetric stretch vibrations) have been observed with Raman spectroscopy experiments under low resolution by Chang *et al.*[140] In Table V we collected information on these bands centres, were "D" in the 3rd column stands for dark upper states in high-resolution ro-vibration spectra analyses and "L" for low resolution Raman experiments, which have not been rotationally resolved.

According to estimations of original analyses of the corresponding experimental data (references listed in 7th column of Table V) the determinations of band centres were much less accurate than in the case of directly observed rotationally resolved bands in high-resolution spectra (Table IV). The experimental accuracy of band centres included in Table V was estimated[19,55,140] in average as 1-3 cm^{-1}. Our *ab initio* calculations are globally within the experimental accuracy for these bands: the RMS deviations is 1.9 cm^{-1} for atomic masses and 1.7 cm^{-1} for nuclear masses, mean deviations being of 0.9 cm^{-1} and 0.1 cm^{-1} correspondingly.

A more detailed comparison of all band centres both with atomic and nuclear masses up to 8000 cm^{-1} calculated using NR_PES is given in the supplementary material[141] (Appendix A3). The lowest $J = 1$ rovibrational levels of A_1 symmetry type allowed by spin statistics for B_1-type vibrations are given in Appendix A4.

The R_PES version appeared to be less successful as far as vibrational predictions are concerned as the errors in vibrational energies were much more significant. In contrast to the NR_PES discussed above the RMS error of vibrational band centers in case of the R_PES version exceeds 9 cm^{-1} both with atomic and with nuclear masses already for the range below 6000 cm^{-1}, the errors being larger for higher energy range that makes some assignments uncertain. The corresponding calculations are given in Appendix A5 of the supplementary material.[141]

VIII. DISCUSSION

In this work we explored the impact of the oxygen basis set and of the shape of the ozone PES near TS towards the dissociation on vibration band centres via first principle calculations. New analytical PES model ((3)-(12)) is proposed

TABLE III. Vibration band centres of $^{16}O_3$ predicted from NR_PES using atomic masses.[a]

$(N' = 0, A_1) \rightarrow (N, A_1)$ bands									
N Γ	E_v	N Γ	E_v	N Γ	E_v	N Γ	E_v	N Γ	E_v
2A	700.68	26A	4245.71	50A	5700.92	74A	6662.26	98A	7435.73
3A	1103.12	27A	4369.24	51A	5767.71	75A	6668.86	99A	7472.72
4A	1398.76	28A	4390.02	52A	5813.00	76A	6749.63	100A	7481.63
5A	1796.05	29A	4537.85	53A	5885.25	77A	6765.49	101A	7538.26
6A	2056.88	30A	4632.17	54A	5889.07	78A	6817.48	102A	7552.44
7A	2094.23	31A	4642.93	55A	5970.11	79A	6869.66	103A	7554.87
8A	2200.92	32A	4707.84	56A	5992.19	80A	6883.47	104A	7600.98
9A	2486.17	33A	4782.14	57A	6013.14	81A	6918.50	105A	7608.68
10A	2724.77	34A	4848.75	58A	6044.71	82A	6929.39	106A	7658.29
11A	2787.02	35A	4919.24	59A	6099.29	83A	6965.30	107A	7685.67
12A	2885.80	36A	4923.55	60A	6155.53	84A	6999.01	108A	7715.90
13A	3083.60	37A	5035.63	61A	6204.11	85A	7074.49	109A	7716.54
14A	3173.35	38A	5038.14	62A	6208.45	86A	7108.43	110A	7783.00
15A	3289.51	39A	5171.31	63A	6239.03	87A	7123.88	111A	7808.09
16A	3389.26	40A	5214.19	64A	6319.50	88A	7149.78	112A	7815.09
17A	3477.09	41A	5264.50	65A	6343.95	89A	7201.16	113A	7836.70
18A	3567.56	42A	5309.39	66A	6365.96	90A	7223.83	114A	7841.40
19A	3739.15	43A	5361.99	67A	6443.32	91A	7224.68	115A	7866.89
20A	3857.36	44A	5417.15	68A	6500.75	92A	7234.09	116A	7890.80
21A	3966.16	45A	5439.73	69A	6505.56	93A	7290.34	117A	7943.73
22A	4000.53	46A	5530.16	70A	6548.86	94A	7310.73	118A	7949.28
23A	4050.29	47A	5541.79	71A	6566.97	95A	7348.09	119A	7957.30
24A	4140.25	48A	5585.72	72A	6613.26	96A	7367.54	120A	7971.01
25A	4164.36	49A	5678.01	73A	6627.10	97A	7379.54	121A	8032.29
$(N' = 0, A_1) \rightarrow (N, B_1)$ bands									
N Γ	E_v	N Γ	E_v	N Γ	E_v	N Γ	E_v	N Γ	E_v
1B	1041.55	19B	4659.07	37B	5919.11	55B	6827.55	73B	7452.81
2B	1725.70	20B	4782.41	38B	5946.30	56B	6878.58	74B	7485.50
3B	2110.62	21B	4897.06	39B	6063.12	57B	6895.13	75B	7518.01
4B	2406.82	22B	4919.22	40B	6084.61	58B	6898.05	76B	7577.97
5B	2784.88	23B	4989.23	41B	6125.00	59B	6980.68	77B	7590.40
6B	3044.88	24B	5074.96	42B	6197.50	60B	6990.22	78B	7617.48
7B	3084.82	25B	5098.41	43B	6266.38	61B	7032.63	79B	7661.90
8B	3185.87	26B	5158.48	44B	6303.59	62B	7075.30	80B	7687.22
9B	3455.29	27B	5291.19	45B	6354.76	63B	7079.58	81B	7722.71
10B	3696.75	28B	5307.00	46B	6388.12	64B	7133.31	82B	7741.15
11B	3759.55	29B	5437.36	47B	6420.57	65B	7160.26	83B	7758.23
12B	3849.25	30B	5519.22	48B	6426.43	66B	7188.46	84B	7779.18
13B	4022.11	31B	5558.58	49B	6543.39	67B	7288.18	85B	7843.87
14B	4121.36	32B	5629.80	50B	6567.98	68B	7309.82	86B	7863.32
15B	4249.67	33B	5695.20	51B	6588.95	69B	7344.59	87B	7928.76
16B	4344.87	34B	5761.98	52B	6687.05	70B	7347.59	88B	7944.73
17B	4430.82	35B	5785.55	53B	6717.47	71B	7393.58	89B	7971.69
18B	4507.37	36B	5799.54	54B	6721.90	72B	7445.56	90B	7991.66
								91B	8044.45

[a]ZPE = 1443.52 cm^{-1}; band centres E_v are given in cm^{-1}; N, Γ- global upper state assignment (see text).

that allows precise fit of *ab initio* points up to high energies near the dissociation threshold. In the currently accessible ranges of spectroscopic experiments ($r \leq 4.5$ a.u.) the RMS deviations for the fit of our *ab initio* points was only 0.17 cm^{-1} up to $E_{max} = 8000$ cm^{-1} and 0.72 cm^{-1} up to $E_{max} = 10\,000$ cm^{-1} (Table II). The $^{16}O_3$ dissociation energy of our *ab initio* PES $D_0 = 1.0548$ eV ⇔ 8508 cm^{-1} lies between the experimental value $D_0^{obs} = 1.052$ eV ⇔ 8485 cm^{-1} cited in most of previous works[1,27–32] (with reference to Gole and Zare[109]) and recent accurate experimental determination by Ruscic[88,89] $D_0^{obs} = 1.06176$ eV ⇔ 8563.9 cm^{-1} (as quoted in Ref. 33).

The dissociation limit of our PES computed from the equilibrium C_{2V} energy is $D_e = 1.136$ eV ⇔ 9164 cm^{-1}. Accounting for our ZPE($^{16}O_3$) = 1443.5 cm^{-1} (Table III) and for ZPE(O_2) = 787 cm^{-1} one can evaluate the corresponding values due to Gole and Ruscic[109] as $D_e^{obs} = 1.133$ eV ⇔ 9141 cm^{-1} and $D_e^{obs} = 1.443$ eV ⇔ 9220 cm^{-1}. Hence our

TABLE IV. Comparison of $^{16}O_3$ band centres observed in high-resolution spectra with *ab initio* predictions using NR_PES.[a]

A upper N Γ	$(v_1v_2v_3)$	E_v obs	at_m O-C	nuc_m O-C	Ref. obs	N Γ	$(v_1v_2v_3)$	E_v	at_m O-C	nuc_m O-C	Ref. obs
2A	(010)	700.931	0.25	0.16	110	21A	(310)	3966.686	0.52	0.00	19
3A	(100)	1103.137	0.01	− 0.14	110	22A	(004)	4001.314	0.78	0.28	117
4A	(020)	1399.273	0.51	0.32	111	24A	(202)	4141.418	1.16	0.63	118
5A	(110)	1796.262	0.21	− 0.03	110	28A	(122)	4390.463	0.44	− 0.11	19
6A	(002)	2057.891	1.01	0.74	110	30A	(014)	4632.888	0.71	0.13	119
7A	(030)	2094.992	0.76	0.48	111	33A	(212)	4783.461	1.32	0.72	120
8A	(200)	2201.155	0.23	− 0.06	110	36A	(104)	4922.572	− 0.98	− 1.57	127 and 19
9A	(120)	2486.576	0.40	0.07	110	39A	(302)	5172.004	0.69	0.03	121
10A	(012)	2726.107	1.33	0.98	110	47A	(114)	5540.896	− 0.90	− 1.56	122 and 19
12A	(210)	2886.178	0.37	− 0.01	112	51A	(204)	5766.322	− 1.39	− 2.06	19
13A	(102)	3083.703	0.10	− 0.29	113	58A	(034)	6046.076	1.36	0.61	132
14A	(130)	3173.929	0.57	0.15	114	59A	(510)	6100.216	0.93	0.13	132
15A	(300)	3289.930	0.42	− 0.01	113	60A	(124)_1	6154.702	− 0.83	− 1.56	132
16A	(022)	3390.918	1.65	1.22	115	65A	(124)_2	6343.983	0.03	− 0.72	133
18A	(220)	3568.07	0.51	0.04	52	66A	(430)	6365.264	− 0.70	− 1.48	133 and 19
19A	(112)	3739.427	0.27	− 0.20	116	69A	(044)	6506.129	0.56	− 0.21	14
						77A	(242)	6764.789	− 0.71	− 1.51	19
B upper N Γ	$(v_1v_2v_3)$	E_v obs	at_m O-C	nuc_m O-C	Ref. obs	N Γ	$(v_1v_2v_3)$	E_v	at_m O-C	nuc_m O-C	Ref. obs
1B	(001)	1042.084	0.53	0.39	110	30B	(213)	5518.812	− 0.41	− 1.07	122 and 19
2B	(011)	1726.522	0.82	0.59	110	31B	(321)	5559.287	0.71	0.01	52
3B	(101)	2110.784	0.16	− 0.11	110	33B	(015)	5697.323	2.12	1.42	128 and 19
4B	(021)	2407.935	1.11	0.80	110	35B	(105)_1	5783.785	− 1.76	− 2.44	131 and 19
5B	(111)	2785.239	0.36	0.00	112	37B	(133)	5919.161	0.05	− 0.67	136
6B	(003)	3046.088	1.21	0.82	113	38B	(411)	5947.070	0.77	0.02	136
7B	(031)	3086.218	1.40	0.99	114	39B	(105)_2	6063.922	0.80	0.05	132
8B	(201)	3186.411	0.54	0.12	113	41B	(223)	6124.288	− 0.71	− 1.43	132
9B	(121)	3455.824	0.54	0.10	115	42B	(331)	6198.534	1.03	0.25	132
10B	(013)	3698.292	1.55	1.08	116	44B	(025)	6305.047	1.46	0.70	133
12B	(211)	3849.911	0.66	0.16	123	45B	(501)	6355.722	0.96	0.14	133
13B	(103)	4021.850	− 0.26	− 0.76	117	46B	(223)	6386.997	− 1.12	− 1.87	133
14B	(131)	4122.069	0.71	0.18	124	50B	(421)	6567.841	− 0.14	− 0.93	13
15B	(301)	4250.223	0.56	0.01	125	51B	(205)	6586.967	− 1.98	− 2.74	13
16B	(023)	4346.727	1.86	1.31	126	53B	(233)	6716.536	− 0.93	− 1.70	135
18B	(221)	4508.132	0.76	0.18	138	57B	(035)	6895.511	0.38	− 0.42	14
19B	(113)	4658.950	− 0.12	− 0.69	119	59B	(511)	6981.870	1.19	0.31	14
21B	(311)	4897.277	0.22	− 0.40	127 and 19	60B	(233)	6990.069	− 0.15	− 0.98	14
22B	(005)_1	4919.203	− 0.02	− 0.62	127 and 19	64B	(125)	7130.774	− 2.53	− 3.32	14
23B	(033)	4991.36	2.13	1.51	139	67B	(153)	7286.774	− 1.40	− 2.21	14
24B	(005)_2	5077.095	2.14	1.50	129 and 19	71B	(601)	7394.801	1.22	0.28	16
26B	(231)	5159.327	0.85	0.20	139	72B	(351)	7446.095	0.54	− 0.36	16
27B	(123)	5291.170	− 0.02	− 0.66	130	73B	(243)	7452.340	− 0.47	− 1.28	16
28B	(401)	5307.790	0.79	0.10	130	76B	(521)	7578.900	0.93	0.04	16

(A+B) upper	at_m		nuc_m	
N bands	RMS (O-C)	Mean (O-C)	RMS (O-C)	Mean (O-C)
81	0.98	0.38	0.99	− 0.20

[a]Band centres E_v, (O-C) = (Obs-Calc), RMS and mean deviations are given in cm^{-1}; N, Γ– global upper state assignment (see text); (at_m): atomic masses calculations; (nuc_m): nuclear masses calculations; vibration normal mode labels are due to original spectra analyses with some revisions.[19]

PES underestimates the most recent experimental determination for the ozone dissociation threshold by only 0.6%.

Two full dimensional *ab initio* versions of the ozone PES were built in this work: one (R_PES) with the submerged reef structure on the TS towards the dissociation and another one without the reef barrier (NR_PES). The construction of the PESs described in Secs. III–V can be summarised as follows. First, we have computed *ab initio* GS electronic energies on a dense grids of points using ic-MRCI/AVXZ method (*a*1 and *a*5 ansätze) for X = 3, 4, 5, 6 as well as for CBS limit; in these calculations the orbitals have been obtained considering only the ground electronic state. As most of the previous ozone electronic structures studies, these *a*1 and *a*5 calculations showed "reef" structures at the TS towards the

TABLE V. Comparison of $^{16}O_3$ band centres obtained from low resolution spectra and "dark state" analyses with *ab initio* predictions using NR_PES.[a]

N Γ	($v_1v_2v_3$)	T	E_v obs	at_m O-C	nuc_m O-C	Ref. obs	N Γ	($v_1v_2v_3$)	T	E_v obs	at_m O-C	nuc_m O-C	Ref. obs
11A	(040)	D	2787.9	0.9	0.5	112	71A	(304)	D	6566.0	− 1.0	− 1.7	13
17A	(050)	D	3478.0	0.9	0.5	52	75A	(350)	D	6671.2	2.3	1.5	135
20A	(140)	D	3859.0	1.6	1.1	123	76A	(520)	D	6750.9	1.3	0.4	19
26A	(230)	D	4246.7	1.0	0.4	125	78A	(412)	D	6820.2	2.7	1.9	135
27A	(400)	D	4370.3	1.1	0.5	126	82A	(106)	L	6927.0	− 2.4	− 3.2	140
27A	(400)	L	4371.0	1.8	1.2	140	84A	(440)_1	D	6999.0	0.0	− 0.9	13
31A	(320)	D	4643.8	0.9	0.3	119	85A	(440)_2	D	7075.8	1.3	0.4	14
38A	(410)	D	5038.5	0.4	− 0.3	129	87A	(026)	D	7121.9	− 2.0	− 2.8	14
39A	(302)	L	5170.0	− 1.3	− 2.0	140	90A	(502)	L	7227.0	3.2	2.3	140
41A	(024)	D	5266.9	2.4	1.8	130	93A	(360)	D	7289.5	− 0.8	− 1.7	14
42A	(330)	D	5310.5	1.1	0.4	130	97A	(252)	D	7379.5	0.0	− 0.9	14
45A	(500)	L	5443.0	3.3	2.6	140	98A	(530)	D	7436.1	0.4	− 0.6	14
46A	(080)	D	5528.8	− 1.4	− 2.1	122 and 52	99A	(144)	D	7476.2	3.5	2.6	14
50A	(420)	D	5701.6	0.7	− 0.1	128	102A	(700)	D	7552.8	0.4	− 0.6	14
51A	(204)	L	5767.0	− 0.7	− 1.4	140 and 19	102A	(700)	L	7555.0	2.6	1.6	140
52A	(312)	D	5812.6	− 0.4	− 1.1	131	104A	(280)	D	7601.2	0.2	− 0.7	14
55A	(340)	D	5971.1	1.0	0.2	13	105A	(342)	D	7607.8	− 0.9	− 1.8	14
56A	(006)	L	5997.0	4.8	4.1	140 and 83							
61A	(402)	L	6204.0	− 0.1	− 0.9	140	20B	(141)	D	4783.2	0.8	0.2	120
64A	(152)	D	6320.2	0.7	− 0.1	133	40B	(161)	D	6087.8	3.2	2.4	83
68A	(600)	L	6506.0	5.3	4.4	140	63B	(205)	D	7077.8	− 1.8	− 2.7	14

N upper vib states	at_m RMS (O-C)	at_m Mean (O-C)	nuc_m RMS (O-C)	nuc_m Mean (O-C)
41	1.9	0.9	1.7	0.1

[a]Band centres E_v, (O-C) = (Obs-Calc), RMS and mean deviations are given in cm^{-1}; N, Γ- global upper state assignment (see text); (at_m) : atomic masses calculations; (nuc_m) : nuclear masses calculations; vibration normal mode labels are due to original spectra analyses with some revisions of Ref. 19; T: type of data (L = low resolution Raman spectra; D = dark states implicitly determined from perturbations of observed bands), estimations for the average accuracy of experimental determinations[19,55,140] being 1-3 cm^{-1}.

dissociation. From these calculations we deduced *ab initio* harmonic frequencies and plotted their behavior against the increasing cardinal number X in Fig. 2 which were compared with empirical harmonic frequencies in Fig. 2 and also in Table I. Unexpected conclusion of this comparison was that one could not improve vibrational predictions in the "spectroscopically accessible PES range" just by increasing the cardinal number of the basis set over X = 5; in fact the results get worse if X > 5 is used. Therefore, we have constructed first a "hybrid" R_PES in a following way: around main PES well inside the "spectroscopically accessible range" we used the results of calculations with X = 5, and beyond this range we used CBS(5,6) extrapolation in order to provide a correct dissociation threshold. A smoothing procedure of these two sets of points gave the R_PES. Since both ansätze *a*1 and *a*5 show the reef TS structure, R_PES shows the same. Still, this PES and related vibrational predictions (see the supplementary material,[141] Appendices A2 and A5) correspond to the higher level of *ab initio* calculations with respect to previous publications.

However, this procedure was not conceptually satisfactory in view of Figs. 2 and 3 and Table I and we were looking for a more consistent solution. The comparisons given in Figs. 2 and 3 as well as in Table I show a clear correlation between the stretching harmonic frequencies and the height of the reef structure barrier (B). This suggested that the major issue is a more realistic PES description of the TS "reef region." To this end we have used the recent finding by Dawes *et al.*[9] that an inclusion of several electronic states in the ic-MRCI procedure influences the shape of the ground state PES near the TS (Sec. III), though their work was limited to 2D points. We have thus accounted for their 2D modification of the PES shape near the TS using a simple symmetrized stretching 2D correction to our best 3D PES according to Eq. (13). This resulted in new full dimensional NR_PES without a reef structure (Secs. III–V). For this PES version both our and Dawes *et al.*[9] calculations were carried out at complete basis set limits: CBS(5,6) in our case and CBS(T,Q) in Ref. 9. Consequently, we consider our NR_PES combining these calculations as a more consistent one. Contrary to the initial version of calculations (Figs. 2(b) and 2(c) and Table I), for this 3D NR_PES we do not have any more contradictions with experimental frequencies at $X \rightarrow \infty$ because the correction (13) removing the reef structure also makes the stretching PES cut more shallow (Fig. 4(f)), thus stretching frequencies are no more overestimated. As the 2D correction (13) is not angular dependent, this does not significantly modify bending frequencies which benefit from the extrapolation $\omega_2 \rightarrow \omega_2$ (*CBS*(5,6)) by increasing their values (Fig. 2(a)) as discussed in Sec. V.

As a result of this work we provide both "reef" version and "non-reef" version of the PES (given in the supplementary material[141]) for the further ozone studies. Both versions of the PES have right asymptotic behaviour for r_1, $r_2 \rightarrow \infty$

in each of (S_i) sectors, Eq. (2). Figures 6, 9, and 11 show that our PES model assures non-additivity property for the ozone fragmentation (Sec. V) and a correct form of the MEP. Figure 10 confirms that shapes for both our analytical PESs are consistent with the previous finding by Schinke *et al.*[1,20,21] that the ozone TS is quite tight and the PES suddenly opens with respect to the angular coordinates just after the critical MEP region of $r >$ 4-5 a.u. The RMS deviations for the fit of our *ab initio* points for large internuclear distances given in Table II prove that our model is quantitatively correct in the dissociation channels at least for the energies relevant for the low temperature and room temperature kinetics in (S_i) sections of the nuclear coordinate space. The 4D representation (r_1, r_2, θ, U) for the bird's-eye view of the PES is given in Figure 12. An application of these PESs for dynamical calculation could be thus instructive to further investigate an eventual role of the reef barrier on the rate coefficients.

As far as spectroscopy applications are concerned our vibrational predictions suggest that NR_PES version would be preferable. For the first time this version of *ab initio* PES gives the RMS deviation below 1 cm^{-1} between first-principle calculations and all available experimental data for vibration-rotation band centers observed in high-resolution spectra up to ~90% of the dissociation threshold. The average error is only 0.38 cm^{-1} (calculations with atomic masses) or 0.20 cm^{-1} (calculations with nuclear masses) that represents a drastic improvement with respect to other recent *ab initio* calculations.[142,143] For dark vibrational states and low resolution Raman bands our *ab initio* predictions are in average within the margins of experimental errors.

To our knowledge this level of accuracy of *ab initio* calculations was obtained for the first time for a molecule with such a complicated electronic structure. This conclusion has to be confirmed by more experimental results on very highly excited spectral transitions reaching the energies comparable with those of the TS range. Such studies requiring extremely sensitive methods for measuring very weak lines represent a formidable challenge for experimental spectroscopy and spectra analyses. We hope that our vibrational predictions of Table IV (completed by Appendices A3 and A4 given in the supplementary material[141]) could help analysing very complicated CRDS laser spectra currently in progress[13–19] in the spectral range up to 8000 cm^{-1}.

From the theoretical chemistry point of view, the approach used to build the NR_PES employed very accurate methodology: first, it was based on extrapolations to CBS limit therefore error due the one-electron basis should be very small; second, applying the corrections from Dawes' calculation, some of the shortcomings of the ic-MRCI procedure has also been corrected. Still, as in case of the PESs for other molecules with complicated electronic structure, the theoretical procedure includes several approximations. In a previous work[33] we have studied some of these: the effect of core-valence correlations on a limited set of points as well as of atomic spin-orbit effect at very large r (with the zero-field splitting of the oxygen atom contributing about 78 cm^{-1} to the dissociation limit) this was not yet included in our full-dimensional PESs. Also the 2D correction (13) was constructed from simple valence 1D cuts[9] interpolated to the equilibrium range. All these approximations could explain small remaining errors for vibrational levels.

We plan a further extension of this study in the following directions. The analytical PES representation ((3)-(12)) is valid only in each of ($s1$), ($s2$), ($s3$) sectors of the coordinate space in the range of $O - \tilde{O} - O$ angles between 85° and 170° excluding the ring D_{3h} structure near $r_1 \sim r_2 \sim r_3 \sim 2.72$ a.u. A global PES appropriate for isotopic exchange reactions could be built from our 3D results by cyclic $r_i \rightarrow r_j \rightarrow r_k$ symmetry permutations with smoothing the barriers among the ($s1$), ($s2$), ($s3$) sectors. We hope that new PES will allow more accurate study of the intra-molecular energy transfer and energy localisation phenomena related to various bifurcations and couplings of vibration-rotation modes.[8,144–146] Other important applications are related to more reliable predictions of metastable ozone states above the dissociation limit in order to find the ground electronic "doorway" states for the dissociation from the first excited electronic state.[18] This would require a non-trivial study for the vibrational basis convergence. Finally, the role of mass dependent corrections beyond the Born-Oppenheimer approximation will be considered as accurate calculations of vibration-rotation levels for various ozone isotopologues could be relevant for the understanding of the puzzling issues of isotopic ozone anomalies.[1–7]

ACKNOWLEDGMENTS

We acknowledge the support from ANR "IDEO" and LEFE-CHAT CNRS grants, from Balaton French-Hungarian PHC exchange program, from IDRIS/CINES computer centers of France and of the computer center "Clovis" Reims-Champagne-Ardenne Region of France. P.G.S. was supported by OTKA F72423 and French-Hungarian intergovernmental Grant No. TeT_11_2_2012_026. We are indebted to T. Muller and R. Schinke for discussions on quantum chemistry calculations as well as to D. Schwenke, M. Jacon, and M. Rey for collaboration in variational methods. Our special thanks are for A. Barbe, E. Starikova, S. Mikhailenko, M. R. De Backer, X. Thomas, A. Campargue, S. Kassi, D. Mondelain, R. Jost, and C. Janssen for stimulating works on ozone spectra measurements and analyses.

[1] R. Schinke, S. Y. Grebenshchikov, M. V. Ivanov, and P. Fleurat-Lessard, Annu. Rev. Phys. Chem. **57**, 625 (2006).
[2] K. Mauersberger, D. Krankowsky, C. Janssen, and R. Schinke, Opt. Phys. **50**, 1 (2005); D. Krankowsky and K. Mauersberger, Science **274**, 1324 (1996).
[3] M. H. Thiemens, Science **293**, 226 (2001); Annu. Rev. Earth Planet Sci. **34**, 217 (2006).
[4] H. Hippler, R. Rahn, and J. Troe, J. Chem. Phys. **93**, 6560 (1990)
[5] C. Janssen, J. Guenther, D. Krankowsky, and K. Mauersberger, Chem. Phys. Lett. **367**, 34 (2003).
[6] Y. Q. Gao and R. A. Marcus, Science **293**, 259 (2001); J. Chem. Phys. **116**, 137 (2002).
[7] R. A. Marcus, J. Chem. Phys. **121**, 8201 (2004); B. C. Hathorn and R. A. Marcus, *ibid.* **111**, 4087 (1999); **113**, 9497 (2000).
[8] S. Y. Grebenshchikov and R. J. Schinke, J. Chem. Phys. **131**, 181103 (2009).
[9] R. Dawes, P. Lolur, J. Ma, and H. Guo, J. Chem. Phys. **135**, 081102 (2011).
[10] D. Babikov, B. K. Kendrick, R. B. Walker, R. T. Pack, P. Fleurat-Lessard, and R. J. Schinke, J. Chem. Phys. **118**, 6298 (2003).

[11]M. V. Ivanov, S. Y. Grebenshchikov, and R. Schinke, J. Chem. Phys. **130**, 174311 (2009); M. V. Ivanov and D. Babikov, *ibid.* **134**, 144107 (2011).
[12]S. Kassi and A. Campargue, J. Chem. Phys. **137**, 234201 (2012).
[13]A. Campargue, A. Barbe, M.-R. De Backer-Barilly, Vl. G. Tyuterev, and S. Kassi, Phys. Chem. Chem. Phys. **10**, 2925 (2008).
[14]A. Barbe, M.-R. De Backer-Barilly, Vl. G. Tyuterev, S. Kassi, and A. Campargue, J. Mol. Spectrosc. **269**, 175 (2011).
[15]E. Starikova, A. Barbe, M.-R. De Backer-Barilly, Vl. G. Tyuterev, S. A. Tashkun, S. Kassi, and A. Campargue, Chem. Phys. Lett. **470**, 28 (2009).
[16]M.-R. De Backer-Barilly, A. Barbe, E. Starikova, Vl. G. Tyuterev, S. Kassi, and A. Campargue, J. Mol. Spectrosc. **272**, 43 (2012).
[17]E. Starikova, A. Barbe, M.-R. De Backer-Barilly, Vl. G. Tyuterev, D. Mondelain, S. Kassi, and A. Campargue, J. Quant. Spectrosc. Radiat. Transf. **113**, 1741 (2012).
[18]D. Mondelain, R. Jost, S. Kassi, R. H. Judge, Vl. G. Tyuterev, and A. Campargue, J. Quant. Spectrosc. Radiat. Transf. **113**, 840 (2012).
[19]A. Barbe, S. Mikhailenko, E. Starikova, M.-R. De Backer, Vl. G. Tyuterev, D. Mondelain, S. Kassi, A. Campargue, C. Janssen, S. Tashkun, R. Kochanov, R. Gamache, and J. Orphal, "Ozone spectroscopy in the electronic ground state: High-resolution spectra analyses and update of line parameters since 2003," J. Quant. Spectrosc. Radiat. Transf (published online).
[20]R. Siebert, R. Schinke, and M. Bittererova, Phys. Chem. Chem. Phys. **3**, 1795 (2001).
[21]R. Siebert, P. Fleurat-Lessard, R. Schinke, M. Bittererova, and S. C. J. Farantos, J. Chem. Phys. **116**, 9749 (2002).
[22]Z.-W. Qu, H. Zhu, and R. Schinke, J. Chem. Phys. **123**, 204324 (2005).
[23]S. Xantheas, G. Atchity, S. Elbert, and K. J. Ruedenberg, J. Chem. Phys. **94**, 8054 (1991).
[24]K. Yamashita, K. Morokuma, F. L. Quere, and C. Leforestier, Chem. Phys. Lett. **191**, 515 (1992).
[25]A. Banichevich, S. D. Peyerimhoff, and F. Grein, Chem. Phys. **178**, 155 (1993); A. Banichevich, S. D. Peyerimhoff, J. A. Beswick, and O. Atabek, J. Chem. Phys. **96**, 6580 (1992).
[26]P. Borowski, M. Fischer, P. A. Malmquist, and B. O. Roos, Chem. Phys. Lett. **237**, 195 (1995).
[27]T. Müller, S. S. Xantheas, H. Dachsel, R. J. Harrison, J. Nieplocha, R. Shepard, G. S. Kedziora, and H. Lischka, Chem. Phys. Lett. **293**, 72 (1998).
[28]D. Xie, H. Guo, and K. A. Peterson, J. Chem. Phys. **112**, 8378 (2000).
[29]R. Hernández-Lamoneda, M. R. Salazar, and R. T. Pack, Chem. Phys. Lett. **355**, 478 (2002).
[30]P. Rosmus, P. Palmieri, and R. Schinke, J. Chem. Phys. **117**, 4871 (2002); M. Tashiro and R. Schinke, *ibid.* **119**, 10186 (2003).
[31]R. Schinke and P. J. Fleurat-Lessard, J. Chem. Phys. **121**, 5789 (2004).
[32]P. Fleurat-Lessard, S. Grebenshchikov, R. Siebert, R. Schinke, and N. J. Halberstadt, J. Chem. Phys. **118**, 610 (2003).
[33]F. Holka, P. G. Szalay, T. Müller, and Vl. G. Tyuterev, J. Phys. Chem. A **114**, 9927 (2010).
[34]M. Lepers, B. Bussery-Honvault, and O. Dulieu, J. Chem. Phys. **137**, 234305 (2012).
[35]M. Ayouz and D. Babikov, J. Chem. Phys. **138**, 164311 (2013).
[36]Vl. G. Tyuterev, S. Tashkun, P. Jensen, and A. Barbe, J. Mol. Spectrosc. **198**, 57 (1999).
[37]Vl. G. Tyuterev, S. Tashkun, D. W. Schwenke, P. Jensen, T. Cours, A. Barbe, and M. Jacon, Chem. Phys. Lett. **316**, 271 (2000).
[38]Vl. G. Tyuterev, S. Tashkun, D. W. Schwenke, and A. Barbe, Proc. SPIE **5311**, 176 (2004).
[39]S. Y. Grebenshchikov, R. Schinke, P. Fleurat-Lessard, and M. Joyeux, J. Chem. Phys. **119**, 6512 (2003).
[40]M. Joyeux, S. Y. Grebenshchikov, J. Bredenbeck, R. Schinke, and S. Farantos, Adv. Chem. Phys. **130**, 267 (2005).
[41]M. Ivanov and D. Babikov, J. Chem. Phys. **134**, 174308 (2011).
[42]S. Y. Grebenshchikov, R. Schinke, Z. W. Qu, and H. Zhu, J. Chem. Phys. **124**, 204313 (2006).
[43]Z. W. Qu, H. Zhu, S. Grebenshchikov, R. Schinke, and S. Farantos, J. Chem. Phys. **121**, 11731 (2004); S. Yu. Grebenshchikov and R. Schinke, *ibid.* **126**, 247101 (2007).
[44]S. A. Ndengué, F. Gatti, R. Schinke, H. D. Meyer, and R. Jost, J. Phys. Chem. A **114**, 9855 (2010); S. A. Ndengué, R. Schinke, F. Gatti, H. D. Meyer, and R. Jost, *ibid.* **116**, 12260 (2012).
[45]T. Shiozaki and H. J. Werner, J. Chem. Phys. **134**, 184104 (2011); A. Kalemos and A. Mavridis, *ibid.* **129**, 054312 (2008).
[46]S. Y. Grebenshchikov, Z. W. Qu, and R. Schinke, Phys. Chem. Chem. Phys. **9**, 2044 (2007).
[47]J. Zúñiga, J. A. Picón, A. Bastida, and A. Requena, J. Chem. Phys. **122**, 224319 (2005); **126**, 244305 (2007).
[48]D. Mondelain, A. Campargue, S. Kassi, A. Barbe, E. Starikova, M.-R. De Backer-Barilly, and Vl. G. Tyuterev, J. Quant. Spectrosc. Radiat. Transf. **116**, 49 (2013).
[49]Vl. G. Tyuterev and V. I. Perevalov, Chem. Phys. Lett. **74**, 494 (1980).
[50]M. R. Aliev and J. K. G. Watson, in *Molecular Spectroscopy: Modern Reseach*, edited by K. Narahari Rao (Acadmic Press, Orlando, FL, 1985), Vol. 3.
[51]Vl. G. Tyuterev, S. A. Tashkun, and H. Seghir, Proc. SPIE **5311**, 164 (2004).
[52]A. Barbe, M.-R. De Backer-Barilly, E. Starikova, S. A. Tashkun, X. Thomas, and Vl. G. Tyuterev, J. Quant. Spectrosc. Radiat. Transf. **113**, 829 (2012).
[53]M. Heyart, A. Perrin, J.-M. Flaud, C. Camy-Peyret, C. P. Rinsland, and M. A. H. Smith, J. Mol. Spectrosc. **157**, 524 (1993).
[54]C. Camy-Peyret, J.-M. Flaud, A. Perrin, V. Malathy Devi, C. P. Rinsland, and M. A. H. Smith, J. Mol. Spectrosc. **118**, 345 (1986).
[55]J.-M. Flaud and R. Bacis, Spectrochim. Acta, Part A **54**, 3 (1998).
[56]A. Chichery, A. Barbe, Vl. G. Tyuterev, and S. Tashkun, J. Mol. Spectrosc. **205**, 347 (2001).
[57]P. Maksyutenko, T. R. Rizzo, and O. V. Boyarkin, J. Chem. Phys. **125**, 181101 (2006); M. Grechko, P. Maksyutenko, T. R. Rizzo, and O. V. Boyarkin, *ibid.* **133**, 081103 (2010).
[58]G. Funke, M. López-Puertas, M. García-Comas, M. Kaufmann, M. Höpfner, and G. P. Stiller, J. Quant. Spectrosc. Radiat. Transf. **113**, 1771 (2012).
[59]R. O. Manuilova, O. A. Gusev, A. A. Kutepov, T. von Clarmann, H. Oelhaf, G. P. Stiller, A. Wegner, M. Lopez-Puertas, F. J. Martin-Torres, G. Zaragoza, and J.-M. Flaud, J. Quant. Spectrosc. Radiat. Transf. **59**, 405 (1998).
[60]H. Partridge and D. W. Schwenke, J. Chem. Phys. **106**, 4618 (1997).
[61]D. W. Schwenke and H. Partridge, J. Chem. Phys. **113**, 6592 (2000).
[62]T. Cours, P. Rosmus, and Vl. G. Tyuterev, J. Chem. Phys. **117**, 5192 (2002).
[63]Vl. G. Tyuterev, L. Regalia Jarlot, D. W. Schwenke, S. A. Tashkun, and Y. G. Borkov, C. R. Phys. **5**, 189 (2004).
[64]L. Lodi, R. N. Tolchenov, J. Tennyson, A. E. Lynas-Gray, S. V. Shirin, N. F. Zobov, O. L. Polyansky, A. G. Császár, J. N. van Stralen, and L. Visscher, J. Chem. Phys. **128**, 044304 (2008).
[65]A. Nikitin, F. Holka, Vl. G. Tyuterev, and J. Fremont, J. Chem. Phys. **130**, 244312 (2009).
[66]S. N. Yurchenko, J. Zheng, H. Lin, P. Jensen, and W. Thiel, J. Chem. Phys. **123**, 134308 (2005).
[67]X. Huang, D. W. Schwenke, and T. J. Lee, J. Phys. Chem. A **113**, 11954 (2009).
[68]S. Carter, A. R. Sharma, J. Bowman, P. Rosmus, and R. Tarroni, J. Chem. Phys. **131**, 224106 (2009).
[69]P. Barletta, S. V. Shirin, N. F. Zobov, O. L. Polyansky, J. Tennyson, E. F. Valeev, and A. G. Császár, J. Chem. Phys. **125**, 204307 (2006).
[70]P. G. Szalay, F. Holka, J. Fremont, M. Rey, K. Peterson, and V. G. Tyuterev, Phys. Chem. Chem. Phys. **13**, 3654 (2011).
[71]F. Holka, P. G. Szalay, J. Fremont, M. Rey, K. Peterson, and V. G. Tyuterev, J. Chem. Phys. **134**, 094306 (2011).
[72]M. Pavanello, L. Adamowicz, A. Alijah, N. F. Zobov, I. I. Mizus, O. L. Polyansky, J. Tennyson, T. Szidarovszky, and A. G. Császár, J. Chem. Phys. **136**, 184303 (2012).
[73]A. V. Nikitin, M. Rey, and Vl. G. Tyuterev, Chem. Phys. Lett. **501**, 179 (2011).
[74]X. Huang, D. W. Schwenke, and T. J. Lee, J. Chem. Phys. **134**, 044320 (2011).
[75]M. Rey, A. V. Nikitin, and Vl. G. Tyuterev, Phys. Chem. Chem. Phys. **15**, 10049 (2013).
[76]P. G. Szalay, T. Müller, G. Gidofalvi, H. Lischka, and R. Shepard, Chem. Rev. **112**, 108 (2012).
[77]P. G. Szalay and R. J. Bartlett, Chem. Phys. Lett. **214**, 481 (1993); J. Chem. Phys. **103**, 3600 (1995).
[78]H.-J. Werner and E. A. Reinsch, J. Chem. Phys. **76**, 3144 (1982); **89**, 5803 (1988).
[79]K. R. Shamasundar, G. Knizia, and H.-J. Werner, J. Chem. Phys. **135**, 054101 (2011).

[80]T. H. Dunning, Jr., J. Chem. Phys. **90**, 1007 (1989); **53**, 2823–2833 (1970).
[81]E. R. Davidson, *The World of Quantum Chemistry*, edited by R. Daudel and B. Pullman (Reidel, Dodrecht, 1974).
[82]EMSL Basis Set Exchange Library, https://bse.pnl.gov/bse/portal; A. K. Wilson, T. van Mourik, and T. H. Dunning, Jr., J. Mol. Struct. **388**, 339 (1997).
[83]H.-J. Werner, P. J. Knowles, R. Lindh, F. R. Manby, M. Schütz *et al.*, MOLPRO, version 2009.1, a package of *ab initio* programs, 2009, see http://www.molpro.net.
[84]W. Kutzelnigg and J. D. Morgan, J. Chem. Phys. **96**, 4484 (1992).
[85]T. Helgaker, W. Klopper, H. Koch, and J. Noga, J. Chem. Phys. **106**, 9639 (1997); A. Halkier, T. Helgaker, P. Jørgensen, W. Klopper, H. Koch, and J. Olsen, Chem. Phys. Lett. **286**, 243 (1998).
[86]E. B. Wilson, J. C. Decius, and P. C. Cross, *Molecular Vibrations* (McGraw-Hill New York, 1955).
[87]A. Barbe, A. Chichery, T. Cours, Vl. G. Tyuterev, and J.-J. Plateaux, J. Mol. Struct. **616**, 55 (2002).
[88]B. Ruscic, R. E. Pinzon, M. L. Morton, G. von Laszewski, S. Bittner, S. G. Nijsure, K. A. Amin, M. Minkoff, and A. F. Wagner, J. Chem. Phys. **108**, 9979 (2004).
[89]B. Ruscic, R. E. Pinzon, M. L. Morton, M.-C. Su, N. K. Srinivasan, J. W. Sutherland, and J. V. Michael, J. Chem. Phys. **110**, 6592 (2006); B. Ruscic, unpublished results obtained from active thermochemical tables (ATcT) based on the Core (Argonne) Thermochemical Network version 1.110 (2010).
[90]M. P. Deskevich, D. J. Nesbitt, and H.-J. Werner, J. Chem. Phys. **120**, 7281 (2004); R. Dawes, A. W. Jasper, C. Tao, C. Richmond, C. Mukarakate, S. H. Kable, and S. A. Reid, J. Phys. Chem. Lett. **1**, 641 (2010).
[91]T. Müller and J. George, private communication (2012).
[92]J. N. Murrell, S. Carter, S. C. Farantos, P. Huxley, and A. J. C. Varandas, *Molecular Potential Energy Function* (Wiley, Chichester, 1984).
[93]P. Jensen, J. Mol. Spectrosc. **133**, 438 (1989); O. L. Polyansky, Per Jensen, and J. Tennyson, J. Chem. Phys. **105**, 6490–6497 (1996).
[94]P. Jensen, S. A. Tashkun, and Vl. G. Tyuterev, J. Mol. Spectrosc. **168**, 271 (1994); R. Guérout, P. R. Bunker, P. Jensen, and W. P. Kraemer, J. Chem. Phys. **123**, 244312-1–244312-8 (2005).
[95]B. J. Braams and J. M. Bowman, Int. Rev. Phys. Chem. **28**, 577 (2009); B. Fu, E. Kamarchik, and J. M. Bowman, J. Chem. Phys. **133**, 164306 (2010).
[96]S. Carter, I. M. Mills, J. N. Murrell, and A. J. C. Varandas, Mol. Phys. **45**, 1053 (1982).
[97]A. J. C. Varandas and J. N. Murrell, Chem. Phys. Lett. **88**, 1 (1982).
[98]A. J. C. Varandas and A. A. C. C. Pais, Mol. Phys. **65**, 843 (1988).
[99]G. Henkelman, G. Jóhannesson, and H. Jónsson, in *Progress in Theoretical Chemistry and Physics*, edited by S. D. Schwartz (Khover-Academic Publishers, The Netherlands, 2002), Vol. 5, p. 269.
[100]G. Henkelman and H. Jónsson, J. Chem. Phys. **111**, 7010 (1999).
[101]D. Sheppard, R. Terrell, and G. Henkelman, J. Chem. Phys. **128**, 134106 (2008).
[102]Obtained from the JANAF reference, M. W. Chase, Jr., C. A. Davies, J. R. Downey, Jr., D. J. Frurip, R. A. McDonald, and A. N. Syverud, J. Phys. Chem. Ref. Data Suppl. **14**, 1 (1985).
[103]J. C. Light and Z. Bacic, J. Chem. Phys. **87**, 4008 (1987); S. Choi and J. Light, *ibid.* **97**, 7031 (1992).
[104]J. Tennyson and J. R. Henderson, J. Chem. Phys. **91**, 3815 (1989); E. Vilanove and M. Jacon, Int. J. Quantum Chem. **62**, 199 (1997).
[105]V. Kokoouline, O. Dulieu, R. Kosloff, and F. Masnou-Seeuws, J. Chem. Phys. **110**, 9865 (1999).
[106]R. G. Littlejohn, M. Cargo, T. Carrington, K. A. Mitchell, and B. Poirier, J. Chem. Phys. **116**, 8691 (2002).
[107]V. A. Mandelshtam and H. S. Taylor, J. Chem. Phys. **106**, 5085 (1997).
[108]V. A. Mandelshtam, T. P. Grozdanov, and H. S. Taylor, J. Chem. Phys. **103**, 10074 (1995).
[109]J. L. Gole and R. N. Zare, J. Chem. Phys. **57**, 5331 (1972).
[110]J.-M. Flaud, C. Camy-Peyret, C. P. Rinsland, M. A. H. Smith, and V. Malathy-Devi (Academic Press, New York, 1990).
[111]A. Barbe, A. Chichery, Vl. G. Tyuterev, S. Taskhun, and S. Mikhailenko, Spectrochim. Acta, Part A **54**, 1935 (1998).
[112]S. N. Mikhailenko, A. Barbe, J.-J. Plateaux, and Vl. G. Tyuterev, J. Mol. Spectrosc. **196**, 93 (1999).
[113]S. Bouazza, A. Barbe, J.-J. Plateaux, J.-M. Flaud, and C. Camy-Peyret, J. Mol. Spectrosc. **160**, 371 (1993).
[114]A. Barbe, S. Mikhailenko, J.-J. Plateaux, and Vl. G. Tyuterev, J. Mol. Spectrosc. **187**, 70 (1998).
[115]S. Bouazza, A. Barbe, S. Mikhailenko, and J.-J. Plateaux, J. Mol. Spectrosc. **166**, 365 (1994).
[116]S. Bouazza, S. Mikhailenko, A. Barbe, L. Regalia, Vl. G. Tyuterev, and J.-J. Plateaux, J. Mol. Spectrosc. **174**, 510 (1995).
[117]J.-M. Flaud, C. Camy-Peyret, A. Perrin, V. Malathy-Devi, A. Barbe, S. Bouazza, J.-J. Plateaux, C. P. Rinsland, M. A. H. Smith, and A. Goldman, J. Mol. Spectrosc. **160**, 378 (1993).
[118]A. Barbe and J.-J. Plateaux, J. Quant. Spectrosc. Raidat. Transf. **55**, 449 (1996).
[119]S. Mikhailenko, A. Barbe, Vl. G. Tyuterev, L. Regalia, and J.-J. Plateaux, J. Mol. Spectrosc. **180**, 227 (1996).
[120]A. Barbe, S. Mikhailenko, J.-J. Plateaux, and Vl. G. Tyuterev, J. Mol. Spectrosc. **182**, 333 (1997).
[121]M. R. De Backer-Barilly, A. Barbe, and Vl. G. Tyuterev, Mol. Phys. **102**, 1707 (2004).
[122]A. Barbe, A. Chichery, Vl. G. Tyuterev, S. Tashkun, and S. Mikhailenko, J. Phys. B **31**, 2559 (1998).
[123]S. Bouazza, A. Barbe, and J.-J. Plateaux, J. Mol. Spectrosc. **171**, 86 (1995).
[124]A. Barbe, S. Mikhailenko, and J.-J. Plateaux, J. Mol. Spectrosc. **184**, 448 (1997).
[125]A. Barbe, O. Sulakshina, J.-J. Plateaux, Vl. G. Tyuterev, and S. Bouazza, J. Mol. Spectrosc. **175**, 296 (1996).
[126]A. Barbe, S. Bouazza, J.-J. Plateaux, and M. Jacon, J. Mol. Spectrosc. **162**, 335 (1993).
[127]J.-M. Flaud, A. Barbe, C. Camy-Peyret, and J.-J. Plateaux, J. Mol. Spectrosc. **177**, 34 (1996).
[128]A. Barbe and C. Chichery, J. Mol. Spectrosc. **192**, 102 (1998).
[129]A. Barbe, J.-J. Plateaux, Vl. G. Tyuterev, and S. Mikhailenko, J. Quant. Spectrosc. Radiat. Transf. **59**, 185 (1998).
[130]A. Barbe, J.-J. Plateaux, S. Mikhailenko, and Vl. G. Tyuterev, J. Mol. Spectrosc. **185**, 408 (1997).
[131]A. Chichery, A. Barbe, Vl. G. Tyuterev, and J.-J. Plateaux, Mol. Phys. **94**, 751 (1998).
[132]A. Barbe, M.-R. De Backer-Barilly, Vl. G. Tyuterev, A. Campargue, D. Romanini, and S. Kassi, J. Mol. Spectrosc. **242**, 156 (2007).
[133]A. Barbe, M.-R. De Backer-Barilly, S. Kassi, and A. Campargue, J. Mol. Spectrosc. **246**, 22 (2007).
[134]A. Barbe, J. J. Plateaux, S. Bouazza, O. N. Sulakshina, S. N. Mikhailenko, Vl. G. Tyuterev, and S. A. Tashkun, J. Quant. Spectrosc. Radiat. Transf. **52**, 341 (1994).
[135]A. Campargue, D. Romanini, S. Kassi, A. Barbe, M.-R. De Backer-Barilly, and Vl. G. Tyuterev, J. Mol. Spectrosc. **240**, 1 (2006).
[136]S. Kassi, A. Campargue, M.-R. De Backer-Barilly, and A. Barbe, J. Mol. Spectrosc. **244**, 122 (2007).
[137]E. Starikova, A. Barbe, D. Mondelain, S. Kassi, A. Campargue, M.-R. De Backer, and Vl. G. Tyuterev, J. Quant. Spectrosc. Radiat. Transf. **119**, 104 (2013).
[138]A. Barbe, S. Mikhailenko, Vl. G. Tyuterev, A. Hamdouni, and J. J. Plateaux, J. Mol. Spectrosc. **171**, 583 (1995).
[139]A. Barbe, private communication (2013)
[140]B. Y. Chang, C. Y. Kung, C. Kittrell, C. W. Hsio, B. R. Johnson, S. G. Glogover, and J. L. Kinsey, J. Chem. Phys. **101**, 1914 (1994).
[141]See supplementary material at http://dx.doi.org/10.1063/1.4821638 for NR_PES and R_PES parameters, corresponding full lists of the calculated band centres for $^{16}O_3$ in the range 0–8000 cm^{-1} as well as $J = 1$ vibration-rotation levels allowed by spin statistics for B_1 vibrational states.
[142]O. Hino, T. Kinoshita, G. K. L. Chan, and R. J. Bartlett, J. Chem. Phys. **124**, 114311 (2006).
[143]A. Karton and J. M. L. Martin, J. Chem. Phys. **133**, 144102 (2010).
[144]L. Xiao and M. E. Kellman, J. Chem. Phys. **90**, 6086 (1989); V. Tyng and M. E. Kellman, *ibid.* **131**, 244111 (2009).
[145]F. Mauguiere, Vl. G. Tyuterev, and S. C. Farantos, Chem. Phys. Lett. **494**, 163 (2010); F. Mauguiere, M. Rey, Vl. G. Tyuterev, J. Suarez, and S. C. Farantos, J. Phys. Chem. A **114**, 9836 (2010); F. Mauguiere, S. C. Farantos, J. Suarez, and R. Schinke, J. Chem. Phys. **134**, 244302 (2011).
[146]M. Kryvohuz and R. A. Marcus, J. Chem. Phys. **132**, 224305 (2010).